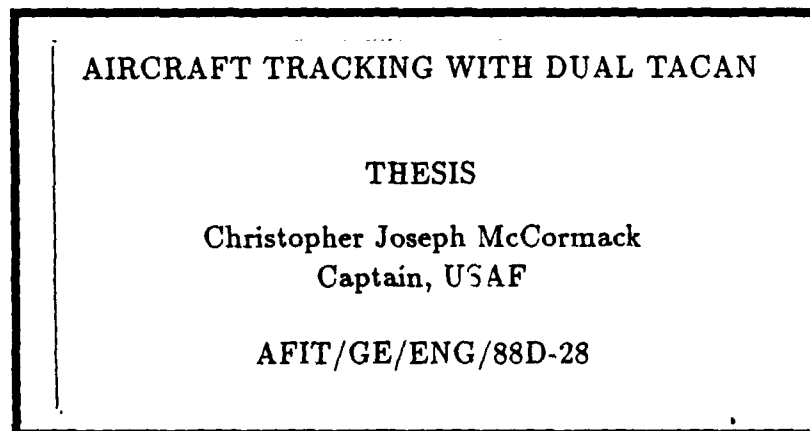


AD-A202 647

DTIC FILE COPY



①  
DTIC  
SELECTED  
17 JAN 1989  
S E D

DEPARTMENT OF THE AIR FORCE  
AIR UNIVERSITY

**AIR FORCE INSTITUTE OF TECHNOLOGY**

Wright-Patterson Air Force Base, Ohio

This document has been approved  
for public release and makes no  
distribution is unlimited.

89

1 17 171

①

AFIT/GE/ENG/88D-28

AIRCRAFT TRACKING WITH DUAL TACAN

THESIS

Christopher Joseph McCormack  
Captain, USAF

AFIT/GE/ENG/88D-28



Approved for Public Release; Distribution Unlimited

**AFIT/GE/ENG/88D-28**

**AIRCRAFT TRACKING WITH DUAL TACAN**

**THESIS**

**Presented to the Faculty of the School of Engineering  
of the Air Force Institute of Technology  
Air University  
In Partial Fulfillment of the  
Requirements for the Degree of  
Master of Science in Electrical Engineering**

**Christopher Joseph McCormack, B.S.**

**Captain, USAF**

**December, 1988**

**Approved for Public Release; Distribution Unlimited**

## *Acknowledgments*

I would like to thank my thesis committee, Capt Williams, LTC Lewantowicz and Dr Maybeck, for all the support and information they provided while I performed this research. They each provided different perspectives to my problems, allowing me to understand how the system would work.

I also want to thank my sponsor, John Franzen, and all the other members of the 4950th Test Wing who helped with this project. They provided the motivation, background information and support that made this a worthwhile undertaking.

Finally, let me express special thanks to my wife [REDACTED] She filled every imaginable role from sounding board and control theory consultant to cheering section and sanity checker. She had her own deadlines to meet, but was always willing to help out when I needed her. While AFIT is tough, going through it with her made it much more bearable.

Christopher Joseph McCormack

Accession For	
NTIS GRA&I	
DTIC TAB	
Unannounced	
Justification	
By _____	
Distribution/ _____	
Availability Codes	
Dist	Avail and/or Special
A-1	



## *Table of Contents*

	Page
<b>Acknowledgments</b> . . . . .	ii
<b>Table of Contents</b> . . . . .	iii
<b>List of Figures</b> . . . . .	vi
<b>List of Tables</b> . . . . .	vii
<b>List of Symbols</b> . . . . .	viii
<b>Abstract</b> . . . . .	xii
<b>I. Introduction</b> . . . . .	1
1.1 Overview . . . . .	1
1.2 Problem Statement . . . . .	2
1.3 Assumptions . . . . .	2
1.4 Standards . . . . .	2
1.5 Scope . . . . .	3
1.6 Approach . . . . .	4
<b>II. Background</b> . . . . .	6
2.1 Overview . . . . .	6
2.2 Navigation and Tracking Systems . . . . .	6
2.3 TACAN Principles . . . . .	7
2.4 TACAN Shortcomings . . . . .	8
2.5 Multiple TACAN Processing . . . . .	10
2.6 Summary . . . . .	11

	Page
<b>III. Model Development . . . . .</b>	<b>12</b>
<b>3.1 Choice of States . . . . .</b>	<b>12</b>
<b>3.2 Measurement Model . . . . .</b>	<b>17</b>
<b>3.3 Summary . . . . .</b>	<b>19</b>
<b>IV. Design and Development . . . . .</b>	<b>20</b>
<b>4.1 Kalman Filters . . . . .</b>	<b>20</b>
<b>4.1.1 Linear Systems . . . . .</b>	<b>20</b>
<b>4.1.2 Nonlinear Systems . . . . .</b>	<b>22</b>
<b>4.2 System Propagation . . . . .</b>	<b>28</b>
<b>4.3 System Updates . . . . .</b>	<b>31</b>
<b>4.4 Optimal Smoothing . . . . .</b>	<b>32</b>
<b>4.4.1 Backward Filter . . . . .</b>	<b>32</b>
<b>4.4.2 Combining Filter Data . . . . .</b>	<b>33</b>
<b>4.5 Programming Environment . . . . .</b>	<b>34</b>
<b>4.6 System Modeling . . . . .</b>	<b>34</b>
<b>4.6.1 Filter Tuning . . . . .</b>	<b>34</b>
<b>V. Computer Simulations . . . . .</b>	<b>37</b>
<b>5.1 Measurement Data Generation . . . . .</b>	<b>37</b>
<b>5.2 Test Scenario . . . . .</b>	<b>37</b>
<b>5.3 System Performance . . . . .</b>	<b>40</b>
<b>5.3.1 Single Simulation Performance . . . . .</b>	<b>40</b>
<b>5.3.2 Monte Carlo Results . . . . .</b>	<b>45</b>
<b>VI. Conclusions and Recommendations . . . . .</b>	<b>49</b>
<b>6.1 System Accuracy . . . . .</b>	<b>49</b>
<b>6.2 Recommendations . . . . .</b>	<b>49</b>
<b>6.3 Follow-On Work . . . . .</b>	<b>49</b>

	Page
6.3.1 Binary Data Files . . . . .	49
6.3.2 Adaptive Extended Kalman Filter . . . . .	50
6.3.3 Factored Filter . . . . .	50
6.3.4 Fine Tuning . . . . .	50
6.3.5 Integration With Wing Data Collection and Reduction . . . . .	50
6.3.6 Multiple Sensor Integration . . . . .	51
Bibliography . . . . .	52
Vita . . . . .	56

## *List of Figures*

<b>Figure</b>		<b>Page</b>
1.	Single TACAN Position Fix . . . . .	8
2.	Single TACAN Positioning Error . . . . .	9
3.	Ideal Triple Range Fix . . . . .	9
4.	Typical Triple Range Fix . . . . .	10
5.	Earth-Centered, Earth-Fixed Coordinate System . . . . .	13
6.	True Bearing to Aircraft . . . . .	19
7.	Test Flight Ground Track . . . . .	38
8.	Test Flight Altitude History . . . . .	39
9.	Test Flight Velocity History . . . . .	39
10.	TACAN Beacon Locations . . . . .	40
11.	Example of X Position Error . . . . .	41
12.	Example of Y Position Error . . . . .	42
13.	Example of Z Position Error . . . . .	42
14.	Example of Radial Error . . . . .	43
15.	Single Smoother Radial Error Cumulative Distribution . . . . .	44
16.	Smoother and Forward Filter Cumulative Error Distributions . . . . .	44
17.	Monte Carlo Results in X Direction . . . . .	45
18.	Monte Carlo Results in Y Direction . . . . .	46
19.	Monte Carlo Results in Z Direction . . . . .	46
20.	Monte Carlo Radial Error . . . . .	47
21.	Cumulative Distribution of Monte Carlo Radial Error . . . . .	47
22.	Cumulative Distribution after t=200 seconds . . . . .	48

*List of Tables*

<b>Table</b>		<b>Page</b>
1.	<b>Tracking System States . . . . .</b>	16
2.	<b>Available Measurements . . . . .</b>	17
3.	<b>Matrix Denominator Terms . . . . .</b>	31
4.	<b>Laplace Transform Pairs . . . . .</b>	31
5.	<b>Driving Noise Strengths . . . . .</b>	35
6.	<b>Measurement Noise Variances . . . . .</b>	35
7.	<b>Creating Simulation Data . . . . .</b>	38

### *List of Symbols*

<b>A</b>	acceleration vector
<i>a</i>	earth radius at equator
$A_x$	x component of acceleration
$A_y$	y component of acceleration
$A_z$	z component of acceleration
<b>B</b>	magnetic bearing
$B_1$	bearing measurement from beacon 1
$B_2$	bearing measurement from beacon 2
<b>B</b>	command input matrix
$BB_1$	bias in bearing measurement 1
$BB_2$	bias in bearing measurement 2
<b>D</b>	down component of range vector
<b>E</b>	east component of range vector
$\epsilon$	earth eccentricity
<b>F</b>	linearized aircraft plant matrix
$f$	earth ellipsoid flattening ratio
<b>G</b>	noise input matrix
$G_d$	discrete noise input matrix
GPS	Global Positioning System
<b>H</b>	measurement model
<i>h</i>	actual aircraft altitude
$h_a$	noise free altimeter value

$h_B$	bias in altimeter measurement
$h_p$	noise corrupted pressure altitude
$J$	intermediate matrix used by backward filter
$K$	Kalman gain matrix
$L$	intermediate matrix used by backward filter
$L$	geodetic latitude
$L_B$	geodetic latitude of TACAN beacon
$L_c$	geocentric latitude
$l$	longitude
$l_B$	longitude of TACAN beacon
LORAN	Long Range Navigation
$M$	intermediate matrix used by backward filter
$N$	north component of range vector
$N_x$	x component of linear estimate in plant matrix
$N_y$	y component of linear estimate in plant matrix
$N_z$	z component of linear estimate in plant matrix
$P$	position vector
$P$	filter covariance matrix
$P_b$	backward filter covariance matrix
$P_x$	x component of aircraft position
$P_y$	y component of aircraft position
$P_z$	z component of aircraft position
$Q$	dynamics driving noise strength matrix
$R$	range between aircraft and beacon
$R_1$	range measurement to beacon 1

$R_2$	range measurement to beacon 2
$R_e$	radial error
$RB_1$	bias in range measurement 1
$RB_2$	bias in range measurement 2
$T_h$	correlation time constant for altimeter
$T$	correlation time constant for acceleration
$t_i$	discrete sample times
TACAN	Tactical Air Navigation
TSPI	Time Space Position Information
$u$	control input vector
$V$	velocity vector (meters/sec)
$V_x$	x component of aircraft velocity
$V_y$	y component of aircraft velocity
$V_z$	z component of aircraft velocity
$v$	measurement noise vector
$v_{B1}$	noise corrupting bearing 1 measurement
$v_{B2}$	noise corrupting bearing 2 measurement
$v_{hp}$	noise corrupting altitude measurement
$v_{R1}$	noise corrupting range 1 measurement
$v_{R2}$	noise corrupting range 2 measurement
var	magnetic variation
$W$	intermediate matrix used for smoother
$w$	driving noise vector
$w_{BB_1}$	bearing bias 1 driving noise
$w_{BB_2}$	bearing bias 2 driving noise

$w_{hB}$	altimeter bias driving noise
$w_{RB_1}$	range bias 1 driving noise
$w_{RB_2}$	range bias 2 driving noise
$\mathbf{X}$	intermediate matrix used for smoother
$\mathbf{x}$	state vector
$\mathbf{x}_b$	backward filter state estimate
$X_B$	x component of TACAN position
$x_t$	true aircraft x position
$\mathbf{Y}$	intermediate matrix used for smoother
$\mathbf{y}_b$	backward filter values
$Y_B$	y component of TACAN position
$y_t$	true aircraft y position
$\mathbf{z}$	measurement vector
$Z_B$	z component of TACAN position
$z_t$	true aircraft z position
$\alpha$	constant based on altimeter time constant
$\beta$	true bearing
$\Phi$	system state transition matrix
$\tau$	constant based on acceleration constant

*Abstract*

This thesis addresses the problem of determining aircraft position during flight given noisy and biased measurements from a barometric altimeter and two tactical air navigation (TACAN) transceivers.

A Kalman smoother is developed to perform post-flight data processing on the measurement data. The smoother estimates aircraft position, velocity, and acceleration as well as biases in the measurements.

Since actual flight test data is not available, computer simulations examine the performance of this tracking technique. The simulated flight includes low and high-speed turns, constant rate ascents, descents, and accelerations. The tracking algorithm tracked the aircraft to within 135 meters of its actual position 95 percent of the time. An unaided inertial navigation system used by the 4950th Test Wing in another flight test program showed a position error growth rate of 2000 meters per hour.

The computer programs which perform the smoothing are written in Fortran-77 and run under the Digital Equipment Corporation VMS operating system.

# AIRCRAFT TRACKING WITH DUAL TACAN

## *I. Introduction*

### *1.1 Overview*

The 4950th Test Wing, located at Wright-Patterson AFB, tests new avionics and electronic warfare equipment for the Air Force. Performance of these systems often varies as the aircraft position changes. While recording test item data during a flight test, the Wing also records Time/Space Position Information (TSPI), a record of the airplane's flight path. TSPI allows Wing data analysts to account for a system's varying performance under test.

The airborne navigation and tracking systems currently available in the 4950th Test Wing do not provide sufficiently accurate TSPI for evaluating test item performance. This inability to record flight path information forces the Test Wing to fly test missions at ranges instrumented with radars to track the airplane. Since Wright-Patterson AFB does not have an instrumented test range, the Wing deploys aircraft and personnel to other bases for test flights.

Deploying aircraft and personnel to test ranges has many drawbacks, including costs for travel, logistical support, and range operating. These additions can easily triple the cost of collecting flight test data. Deploying to a test range can also adversely affect the program schedule. Conflicts over use of range resources arise when programs from different test organizations both require use of range facilities. If the 4950th Test Wing's program has a low Department of Defense priority, it may have to wait for an opportunity to fly on the range.

### ***1.2 Problem Statement***

The 4950th Test Wing needs an inexpensive and accurate aircraft tracking system. The Wing wants to know if optimally combining the signals from two Tactical Air Navigation (TACAN) transceivers can supply this tracking information [21]. This will provide the capability to fly test missions without using a test range radar for tracking support.

### ***1.3 Assumptions***

The Test Wing does not need tracking data displayed in real time on the aircraft. Post flight data analysis allows the use of existing Test Wing computer facilities. A real-time system requires installation of a computer on the aircraft, increasing system cost and complexity.

The aircrew selects TACAN beacons to provide coverage during each flight segment. They decide which TACAN beacons to use while mission planning before the test flight.

The airborne system records station identifiers, ranges, and bearings from TACAN beacons. The system also records the time of day and barometric altitude. This information allows post-flight data processing to calculate a complete three-dimensional time history of the aircraft flight path.

### ***1.4 Standards***

The 4950th Test Wing requires TSPI accurate to within several hundred feet of the actual aircraft position. In addition to meeting this accuracy requirement, the tracking system employed must conduct any necessary pre-flight calibrations rapidly. The delay between equipment power-up and takeoff must be less than 30 minutes. Converting TACAN measurement files into aircraft track files should not slow the analysis of project data. Less than two days of data reduction should provide TSPI data for a two-hour flight.

The track files generated by this system can be formatted to match TSPI files generated at Eglin AFB. This compatibility avoids the need to develop two sets of analysis tools; one for use with dual TACAN data and another for use with test range radar data. Test programs would thus have the flexibility of flying with either source of tracking data.

Since the dual TACAN system cannot provide extremely accurate tracking data, it would not replace all test range flying. Dual TACAN can provide a low-cost alternative for programs not requiring extremely accurate positioning data. Dual TACAN would also allow local flying to verify test system operation before deploying a test team to an instrumented range for more comprehensive flight tests.

If the Dual TACAN system cannot be readily implemented, the Wing will continue to use their current limited tracking ability until the Global Positioning System (GPS) becomes operational and user equipment becomes available. When fully deployed, GPS satellites will allow an aircraft to record its position within 15 meters [19:55]. Dual TACAN can serve as an interim measure until GPS becomes fully operational and the Test Wing installs GPS receivers on their aircraft.

### 1.5 Scope

This project builds upon work already performed in the Test Analysis Branch of the 4950th Test Wing. They have developed a program to take TACAN measurement data and convert it into an aircraft track file. Because of budget and manpower limitations, their programs do not attempt to filter out noise from data. Digitally processing TACAN information with a Kalman filter can remove noises and biases to produce a more accurate track file.

The proposed system uses two AN/ARN-118(V) TACAN transceivers. The AN/ARN-118 serves as the standard TACAN system for Test Wing aircraft [39:3]. Taking additional measurements from a third or fourth TACAN beacon by installing additional transceivers or continuously retuning the available transceivers

can lead to a more accurate tracking system. These additional measurements are not considered in this project because:

1. Installing additional TACAN transceivers is difficult because of:
  - limited available airplane equipment space
  - limited available airplane equipment power
  - requirement to mount additional TACAN antennas externally
2. Manually retuning available transceivers increases the aircrew workload and has the potential for errors and loss of track data.
3. Automatically retuning TACAN transceivers represent costly custom equipment not currently available in the Test Wing.
4. Constantly retuning the airborne transceivers forces the TACAN to operate in an acquisition mode which may last as long as 20 seconds. During this time, the transceiver places an operating load 6 times the standard tracking level on the ground beacon. This can seriously degrade the beacons ability to handle multiple aircraft [7:15].

#### *1.6 Approach*

The initial task in this project involves reviewing technical literature on navigation and signal processing systems. This provided background on how a dual TACAN system can provide tracking data and benefits possible from filtering that data. Chapter II of this thesis summarizes the results of the literature review.

In 1986 and 1987, the 4950th Test Wing performed preliminary work with TACAN tracking. While a lack of funding and manpower prevented completion of the project, the Wing's Test Analysis Division (4950 TESTW/FFT) used computer simulations to analyze a TACAN tracking system's performance [39,17]. These programs are the starting point for this thesis.

This project does not involve any special equipment. AFIT's computer systems provide the development environment for new programs which convert TACAN measurement files into TSPI track files. Program checkout and test data analysis use both AFIT and Test Wing computers.

This analysis requires an accurate model for the TACAN transceiver measurements. Chapter III develops a model for the tracking problem. Chapter IV concentrates on the actual design and development of the tracking software. Chapter V discusses the simulations conducted using the dual TACAN tracker and compares the accuracy of the filter reported position against actual aircraft position. Chapter VI summarizes the project.

## *II. Background*

### *2.1 Overview*

Flight testing new avionics and electronic warfare equipment for the Air Force usually requires accurate knowledge of the aircraft's position throughout the flight. Currently available air navigation systems in the 4950th Test Wing cannot provide this type of information. This forces the Wing to fly their test missions at instrumented test ranges, such as Eglin AFB, FL or Holloman AFB, NM.

The Test Wing would like to have a system on the aircraft capable of providing this positioning data. This system would allow projects to conduct tests without deploying to test ranges.

### *2.2 Navigation and Tracking Systems*

The Test Wing currently has several different navigation systems available to support test programs. All Wing aircraft are equipped with TACAN transceivers. Standard TACAN measurements are not very accurate, and position uncertainties increase with aircraft range from the ground beacon.

The Test Wing also uses Carousel IV-E inertial navigation systems (INS). These are not high-precision INS units by current standards. The Carousel IV-E accuracy specification allows the radial position error to grow at a rate of two nautical miles per hour [39:26].

The satellite-based GPS is the newest system available in the Test Wing. In the near future, the flexibility and high accuracy of GPS will satisfy virtually all of the Wing's aircraft tracking requirements. Unfortunately, airborne GPS equipment is not yet readily available, and all the satellites necessary to support GPS have not been launched [19].

As an interim measure, John Franzen, a data analyst in the 4950th Test Wing, investigated methods to process available navigation data after a flight to obtain more accurate estimates of the aircraft track [15,17,18]. A Test Wing report suggested a TACAN-based system to provide flight path data [39].

### **2.3 TACAN Principles**

Small size, low power requirements, simple operation, and low cost all combine to make TACAN the primary method of aircraft navigation in the United States [19:50]. While the Department of Defense does operate some TACAN sites, the majority of beacons installed in the United States are maintained by the Federal Aviation Administration, a branch of the Department of Transportation.

The airborne TACAN equipment provides two pieces of information to the crew. By transmitting pulses to a ground station and timing the delay before receiving response pulses, the system measures distance between the aircraft and beacon. The system also displays bearing from the beacon to the aircraft based on variations in the beacon's rotating antenna pattern.

Navigation with TACAN involves polar geometry. The airborne equipment displays the aircraft range and bearing from a ground beacon. Beacon locations are displayed on navigation charts, making it simple to determine the airplane's position with a chart, a pair of dividers and a protractor (see Figure 1).

To simplify enroute navigation using TACAN, the Federal Aviation Administration has established airways and jet routes between TACAN beacons. Aircraft fly along these routes from one TACAN to another, using the range measurement to indicate their position in the route and providing an estimate of how long until the next course change.

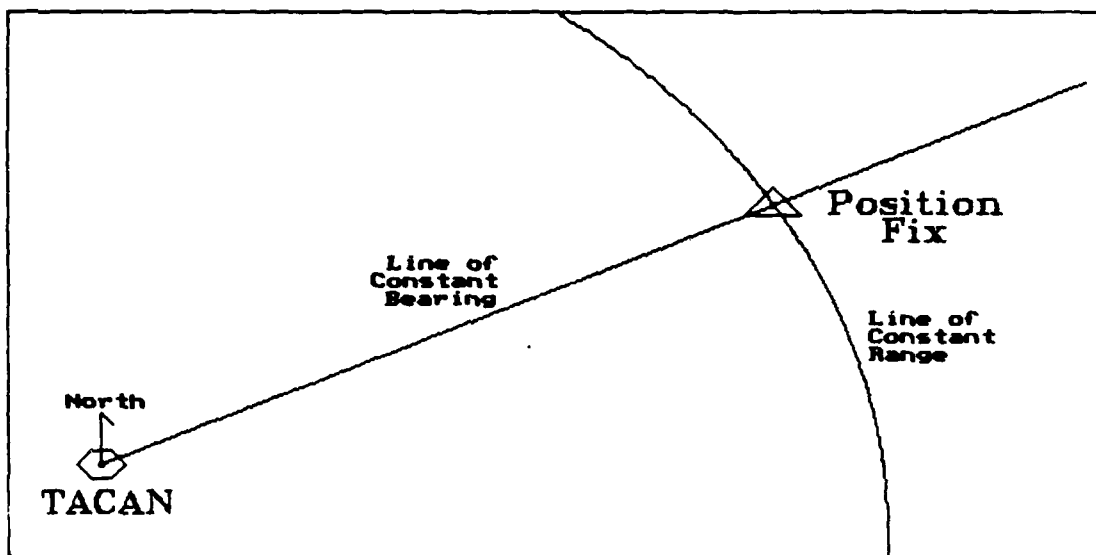


Figure 1. Single TACAN Position Fix

#### 2.4 TACAN Shortcomings

Polar geometry causes TACAN accuracy to decrease as distance to the station increases. The magnitude of typical TACAN measurement errors average 1.65 degrees of bearing error and 600 feet of range error [39:50]. For an aircraft located 30 miles from a TACAN beacon, 1.65 degrees of bearing error and 600 feet of range error represent over 5000 feet of position error (see Figure 2).

Inaccurate bearing information comprises the major error component of TACAN signals. Combining several more accurate range measurements can determine an aircraft's position without using bearing data. Groginsky showed how range measurements to three different ground beacons could provide the position and altitude of an aircraft [22:178]. Figure 3 shows the ideal case of three range measurements providing a position fix. Measurement noises and biases cause the typical situation to resemble Figure 4 with no single unambiguous aircraft position indicated by the measurements.

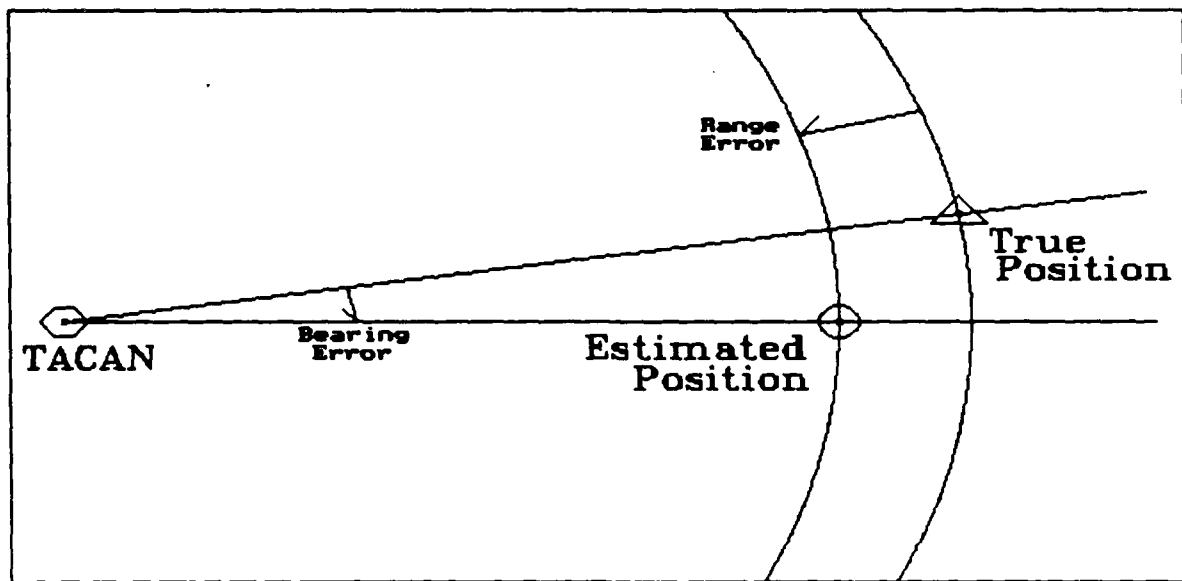


Figure 2. Single TACAN Positioning Error

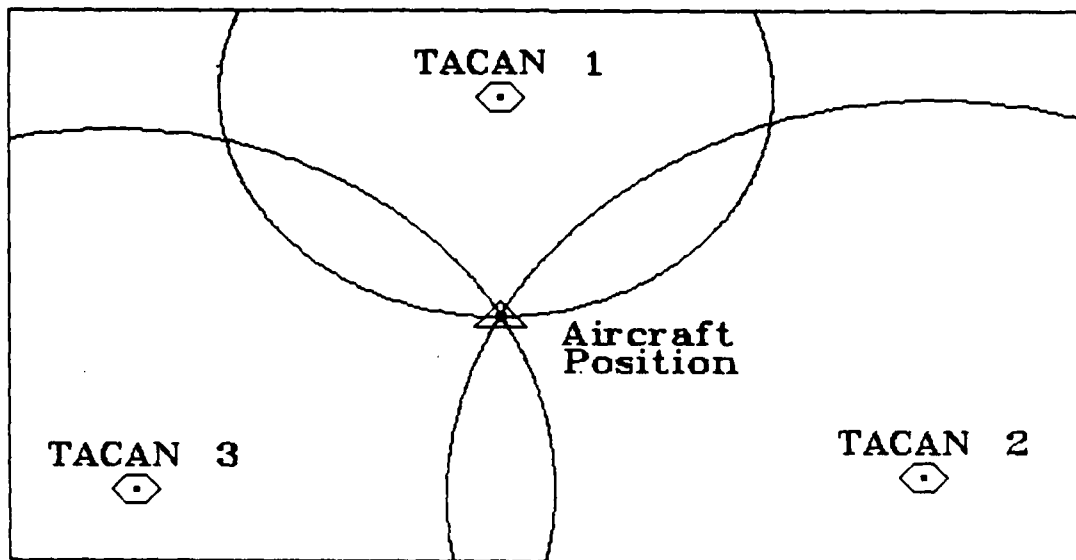


Figure 3. Ideal Triple Range Fix

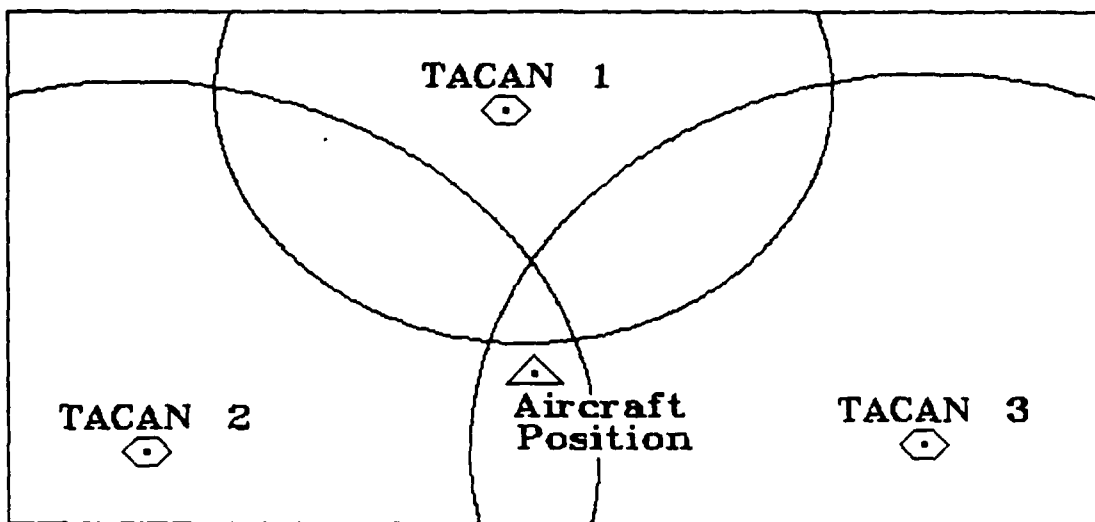


Figure 4. Typical Triple Range Fix

## *2.5 Multiple TACAN Processing*

Multiple range measurements for aircraft positioning served as the basis for Latham's research at Grumman Aerospace Corporation. In a prototype system, Latham combined range data from ten different ground beacons and could consistently calculate an aircraft's position within 200 feet of the actual position [26:157]. Later work added inertial navigation system data for greater accuracy [27:72].

Riggins followed on Latham's work and examined different methods of combining multiple range measurements [47]. The technique developed by Riggins could calculate aircraft position during flight without need for post-flight computer analysis of the range data. This system accurately positioned the aircraft within 200 feet [47:101].

Latham and Riggins used single-channel TACAN systems on-board the aircraft. To obtain multiple range measurements, computers automatically switched the aircraft TACAN transceiver to different ground beacons throughout the flight. Existing Air Force TACAN equipment used in the Test Wing's aircraft cannot perform automatic switching.

Tests conducted by the 4950th Test Wing suggest a different approach to position fixing. The Wing's proposed system would record the output from two separate TACAN transceivers along with the output of a pressure altimeter. These three measurements provide sufficient information to determine aircraft position [44:28].

Analysis of TACAN signals by the Test Wing revealed the potential to extract, with additional signal processing, high accuracy range measurements by removing measurement biases. Error analysis based on measurements of TACAN stations near Wright-Patterson AFB indicate that such a system could accurately position the airplane within 300 feet [39:F7]. After initial analysis of the problem, lack of manpower and funding prevented the Wing from investigating this system further.

Systems currently in development offer tracking capability far exceeding the Test Wing's requirements. The satellite-based GPS will provide position information accurate to within 15 meters [19:55]. Although GPS was scheduled to be fully operational by 1984 [19:55], the seven satellites currently in orbit are pre-production models. The first production satellite will be launched 30 December 1988 with 6 additional satellites added each year for the next three years [20]. At this rate, the 21 satellites necessary for full GPS coverage will not be available until 1991. Even if the satellites were orbiting, airborne GPS receivers are currently expensive and difficult to obtain.

## *2.6 Summary*

Combining the signals from multiple TACAN transceivers offers an opportunity to collect precision tracking data without the need for special equipment. This will improve the Test Wing's in-house tracking capability in an economical manner.

### *III. Model Development*

The system model serves as the heart of any stochastic estimator. The model outlined in this chapter is driven by the available measuring devices and a simplified model of the aircraft dynamics.

#### *3.1 Choice of States*

On-board navigation systems typically access commands entered by the pilot and use this information when estimating aircraft trajectory. The T-39B Sabreliners flown by the 4950th Test Wing have no provisions for measuring or recording this information. Without command inputs, the tracking system resembles a weapon guidance system tracking an uncooperative target.

Aircraft dynamics were divided into three orthogonal, uncoupled Cartesian components. To represent unknown pilot inputs, the model uses three independent white Gaussian noises arranged in a vector denoted as  $w(t)$ . To represent physical maneuvering characteristics of the aircraft more accurately, this input passes through a first-order lag shaping filter with a time constant of  $T$  to correlate input accelerations. Integrating acceleration provides velocity; integrating velocity yields position. This type of dynamics model is often used for non-cooperative aircraft in targeting systems [6,38,47].

Equations (1)–(3) state the scalar version of this model for one dimension:

$$\dot{P}(t) = V(t) \quad (1)$$

$$\dot{V}(t) = A(t) \quad (2)$$

$$\dot{A}(t) = -\frac{1}{T}A(t) + w(t) \quad (3)$$

Repeating the equations in the  $x$ ,  $y$  and  $z$  directions provide nine separate equations, driven by three independent noise sources.

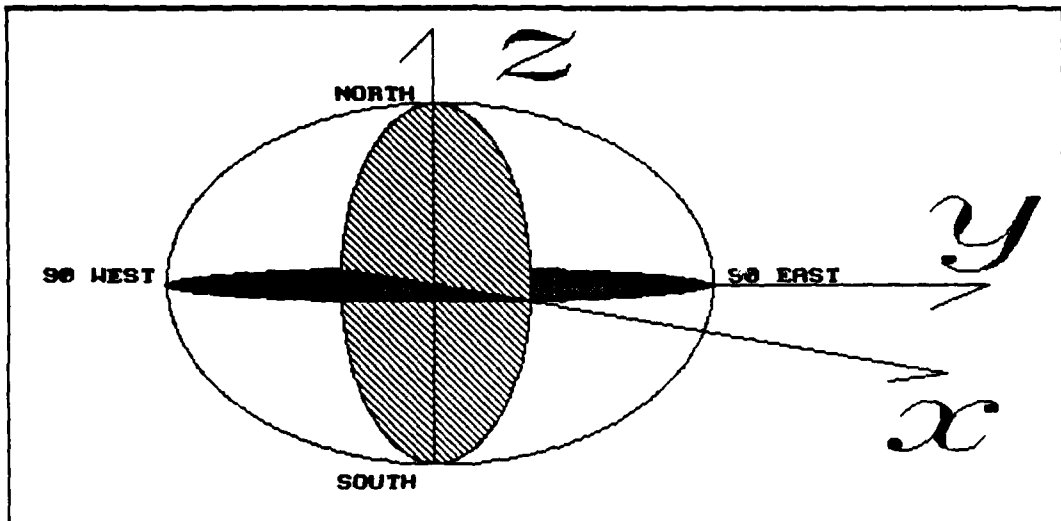


Figure 5. Earth-Centered, Earth-Fixed Coordinate System

The orthogonal  $xyz$  reference frame uses earth-centered, earth-fixed coordinates. This places the origin at the earth's center with the  $x$ -axis pointing out along the equator at the prime meridian, the  $z$ -axis pointing through the north pole, and the  $y$ -axis pointing out along the equator at 90 degrees east longitude to complete a right-handed  $xyz$  coordinate system. Figure 5 shows the earth-centered, earth-fixed coordinate system.

Expressing the position, velocity and acceleration components as a vector differential equation models the aircraft dynamics equations in standard form as a

ninth-order system (with  $\tau$  representing  $-1/T$  to allow more compact equations):

$$\begin{bmatrix} \dot{P}_x \\ \dot{P}_y \\ \dot{P}_z \\ \dot{V}_e \\ \dot{V}_y \\ \dot{V}_z \\ \dot{A}_x \\ \dot{A}_y \\ \dot{A}_z \end{bmatrix} = \begin{bmatrix} 0 & 0 & 0 & 1 & 0 & 0 & 0 & 0 & 0 \\ 0 & 0 & 0 & 0 & 1 & 0 & 0 & 0 & 0 \\ 0 & 0 & 0 & 0 & 0 & 1 & 0 & 0 & 0 \\ 0 & 0 & 0 & 0 & 0 & 0 & 1 & 0 & 0 \\ 0 & 0 & 0 & 0 & 0 & 0 & 0 & 1 & 0 \\ 0 & 0 & 0 & 0 & 0 & 0 & 0 & 0 & 1 \\ 0 & 0 & 0 & 0 & 0 & 0 & 0 & \tau & 0 \\ 0 & 0 & 0 & 0 & 0 & 0 & 0 & 0 & \tau \\ 0 & 0 & 0 & 0 & 0 & 0 & 0 & 0 & 0 \end{bmatrix} \begin{bmatrix} P_x \\ P_y \\ P_z \\ V_e \\ V_y \\ V_z \\ A_x \\ A_y \\ A_z \end{bmatrix} + \begin{bmatrix} 0 & 0 & 0 \\ 0 & 0 & 0 \\ 0 & 0 & 0 \\ 0 & 0 & 0 \\ 0 & 0 & 0 \\ 0 & 0 & 0 \\ 1 & 0 & 0 \\ 0 & 1 & 0 \\ 0 & 0 & 1 \end{bmatrix} \begin{bmatrix} w_x \\ w_y \\ w_z \end{bmatrix} \quad (4)$$

The value  $-(1/4)\text{sec}^{-1}$  used for  $\tau$  corresponds to the acceleration time constant found in a typical non-fighter aircraft [37].

For navigation purposes, the earth is modeled as an ellipsoid with semi-major axis  $a$  and eccentricity  $\epsilon$  [1]. Based upon this reference ellipsoid, transforming geodetic coordinates expressed in latitude, longitude and altitude ( $L, l, h$ ) to earth-centered, earth-fixed coordinates used by the filter ( $P_x, P_y, P_z$ ) is done with:

$$P_x = \left[ \frac{a}{\sqrt{1 - \epsilon^2 \sin^2 L}} + h \right] \cos L \cos l \quad (5)$$

$$P_y = \left[ \frac{a}{\sqrt{1 - \epsilon^2 \sin^2 L}} + h \right] \cos L \sin l \quad (6)$$

$$P_z = \left[ \frac{a(1 - \epsilon^2)}{\sqrt{1 - \epsilon^2 \sin^2 L}} + h \right] \sin L \quad (7)$$

In addition to the nine states already selected, the filter must model characteristics of the measurement sensors. One measurement available to the filter is pressure altitude. Delay in the altitude transducer requires the addition of another state to the filter which accounts for the lag in altimeter output during ascents and descents. The altimeter value depends on the previous altimeter reading and the actual altitude. Altitude is a nonlinear function of the aircraft position vector

$\mathbf{P}$  consisting of the components  $P_x$ ,  $P_y$ ,  $P_z$ . This function gives the length of the vector from the aircraft position perpendicular to the reference geoid.

$$\begin{aligned}\dot{h}_a(t) &= -\frac{1}{T_a} h_a(t) + \frac{1}{T_a} h\{\mathbf{P}(t)\} \\ &= ah_a(t) - ah\{\mathbf{P}(t)\}\end{aligned}\quad (8)$$

Equation (9) shows the nonlinear relationship between the aircraft earth-centered, earth-fixed position and altitude.

$$h = \frac{P_z}{\sin L} - \frac{a(1 - \epsilon^2)}{\sqrt{1 - \epsilon^2 \sin^2 L}} \quad (9)$$

This nonlinearity forces the tracker to use an extended Kalman filter.

Along with altimeter dynamics, all measurements contain biases the filter must estimate and remove. Tests conducted by the 4950th Test Wing and by the British Royal Aircraft Establishment indicate TACAN errors consist of large, slowly varying biases ranging from  $-225$  to  $+340$  meters and small white noise components with approximate covariance of  $400m^2$  [39,45]. This tracking system uses five measurements, each with an unknown bias. These result in filter states for the two range biases ( $RB_1, RB_2$ ), the two bearing biases ( $BB_1, BB_2$ ) and the altimeter bias ( $hB$ ). Each bias state corresponds to the output of an integrator driven by small magnitude, pair-wise uncorrelated noises. The initial values of these integrators are read from a data file based on previous flight tests.

$$\begin{bmatrix} RB_1 \\ BB_1 \\ RB_2 \\ BB_2 \\ hB \end{bmatrix} = \begin{bmatrix} 0 & 0 & 0 & 0 & 0 \\ 0 & 0 & 0 & 0 & 0 \\ 0 & 0 & 0 & 0 & 0 \\ 0 & 0 & 0 & 0 & 0 \\ 0 & 0 & 0 & 0 & 0 \end{bmatrix} \begin{bmatrix} RB_1 \\ BB_1 \\ RB_2 \\ BB_2 \\ hB \end{bmatrix} + \begin{bmatrix} 1 & 0 & 0 & 0 & 0 \\ 0 & 1 & 0 & 0 & 0 \\ 0 & 0 & 1 & 0 & 0 \\ 0 & 0 & 0 & 1 & 0 \\ 0 & 0 & 0 & 0 & 1 \end{bmatrix} \begin{bmatrix} w_{RB_1} \\ w_{BB_1} \\ w_{RB_2} \\ w_{BB_2} \\ w_{hB} \end{bmatrix} \quad (10)$$

When combined, the preceding equations describe a system using the fifteen states shown in Table 1. Since the bias states are independent of position, veloc-

Table 1. Tracking System States

$P_x$	Aircraft Position
$P_y$	
$P_z$	
$V_x$	Aircraft Velocity
$V_y$	
$V_z$	
$A_x$	Aircraft Acceleration
$A_y$	
$A_z$	
$h_a$	Altimeter Output
$RB_1$	TACAN 1 Biases
$BB_1$	
$RB_2$	TACAN 2 Biases
$BB_2$	
$hB$	Altimeter Bias

ity, acceleration or altitude, bias states can be appended to provide the following system representation:

$$\dot{P}_x = V_x \quad (11)$$

$$\dot{P}_y = V_y \quad (12)$$

$$\dot{P}_z = V_z \quad (13)$$

$$\dot{V}_x = A_x \quad (14)$$

$$\dot{V}_y = A_y \quad (15)$$

$$\dot{V}_z = A_z \quad (16)$$

$$\dot{A}_x = -\frac{1}{T}A_x + w_x \quad (17)$$

$$\dot{A}_y = -\frac{1}{T}A_y + w_y \quad (18)$$

$$\dot{A}_z = -\frac{1}{T}A_z + w_z \quad (19)$$

$$\dot{h}_a = -\frac{1}{T_a}h_a + \frac{1}{T_a}h(P_x, P_y, P_z) \quad (20)$$

$$\dot{RB}_1 = w_{RB_1} \quad (21)$$

Table 2. Available Measurements

$R_1$	slant range to beacon 1
$B_1$	magnetic heading from beacon 1 to aircraft
$R_2$	slant range to beacon 2
$B_2$	magnetic heading from beacon 2 to aircraft
$h_p$	pressure altitude measured on aircraft

$$BB_1 = w_{BB_1} \quad (22)$$

$$RB_2 = w_{RB_2} \quad (23)$$

$$BB_2 = w_{BB_2} \quad (24)$$

$$hB = w_{hB} \quad (25)$$

This can be stated more succinctly in matrix form as:

$$\dot{x}(t) = f[x(t)] + G(t)w(t) \quad (26)$$

### 3.2 Measurement Model

Having established the dynamics model for the target aircraft, the next step in designing a filter is to determine the measurement model. The available measurements shown in Table 2 can be related to the fifteen system state variables to establish a measurement model for the state estimator.

The following equations show the relationship between state variables, recorded sampled-data measurements, and the components of the noise vector  $v(t_i)$  entering each measurement. The functions for range and bearing are discussed later in this chapter.

$$R_1 = R_1(P_x, P_y, P_z) + RB_1 + v_{R1} \quad (27)$$

$$B_1 = B_1(P_x, P_y, P_z) + BB_1 + v_{B1} \quad (28)$$

$$R_2 = R_2(P_x, P_y, P_z) + RB_2 + v_{R2} \quad (29)$$

$$B_2 = B_2(P_x, P_y, P_z) + BB_2 + v_{B2} \quad (30)$$

$$h_p = h_a + hB + v_{hp} \quad (31)$$

This set of equations can be rewritten in vector form as:

$$\mathbf{z}(t_i)\mathbf{h}[\mathbf{x}(t_i)] + \mathbf{v}(t_i) \quad (32)$$

The filter knows a priori the earth-centered, earth-fixed coordinates for the TACAN beacons ( $X_B$ ,  $Y_B$  and  $Z_B$ ). Using TACAN position and aircraft coordinates, the following equation gives slant range from the beacon to the aircraft:

$$R = \sqrt{(P_x - X_B)^2 + (P_y - Y_B)^2 + (P_z - Z_B)^2} \quad (33)$$

The filter also uses bearing measurements from the TACANs to the aircraft. These measurements are magnetic bearings based on the local tangent plane defined at the beacon. The range vector between the beacon and the aircraft,  $[(P_x - X_B) (P_y - Y_B) (P_z - Z_B)]^T$ , is projected into a north, east, down coordinate system based on the beacon's geodetic latitude ( $L_B$ ) and longitude ( $l_B$ ). The north, east and down ( $N$ ,  $E$ ,  $D$ ) components of the range vector are given by the vector transformation [4]:

$$\begin{bmatrix} N \\ E \\ D \end{bmatrix} = \begin{bmatrix} -\sin L_B \cos l_B & -\sin L_B \sin l_B & \cos L_B \\ -\sin l_B & \cos l_B & 0 \\ -\cos L_B \cos l_B & -\cos L_B \sin l_B & -\sin L_B \end{bmatrix} \begin{bmatrix} P_x - X_B \\ P_y - Y_B \\ P_z - Z_B \end{bmatrix} \quad (34)$$

After calculating the north and east range vector components, using the inverse tangent gives true heading from the beacon as shown in Figure 6. The magnetic heading reported by the TACAN receiver will also have the local magnetic variation at the beacon added to the true heading. Note that east magnetic variation is added while west magnetic variation is subtracted from the true heading,  $\beta$ , to give magnetic heading,  $B$ .)

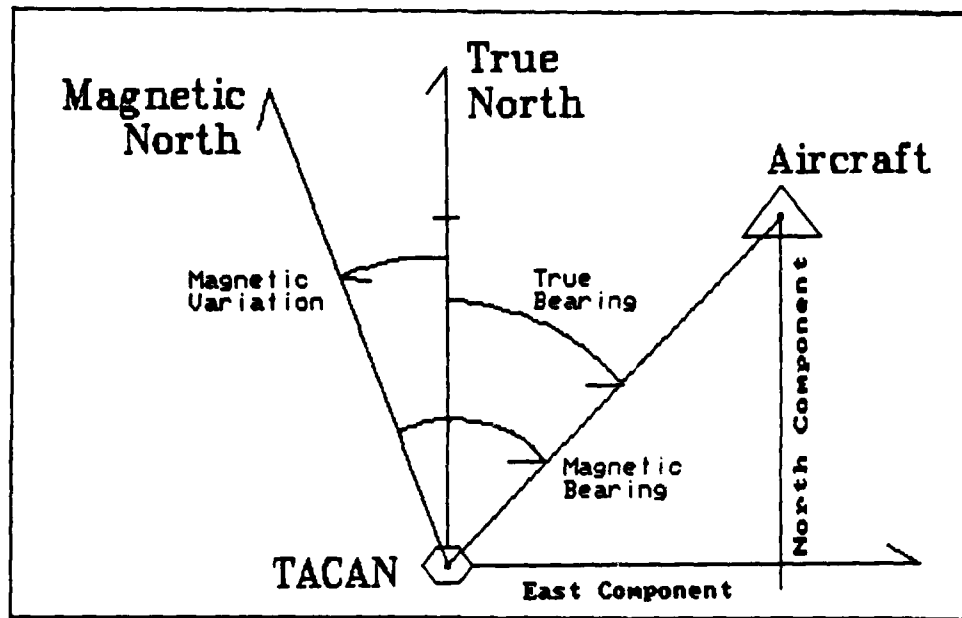


Figure 6. True Bearing to Aircraft

$$\beta = \tan^{-1} \frac{E}{N} \quad (35)$$

$$B = \beta + \text{var} \quad (36)$$

The transformation matrix defined in Equation (34) depends only on beacon coordinates, not aircraft position. A lookup table stores the geographic coordinates and magnetic variation for each TACAN beacon.

### 3.3 Summary

The 15-state dynamics model and the 5-state measurement model discussed in this chapter serve as the foundation for developing a state estimator. The next chapter develops a Kalman filter to process the measurement data and estimate the aircraft position.

## *IV. Design and Development*

The Chapter III measurement and dynamics models serve as the basis for a stochastic estimator which takes noisy measurements and estimates the aircraft flight path.

### *4.1 Kalman Filters*

The tracking system developed in this study uses a Kalman filter to estimate errors in sensor measurements and to allow accurate calculation of aircraft position. A Kalman filter is an optimal recursive data processing algorithm designed to estimate state variables of interest. The filter uses all available measurements, regardless of their precision, as well as a priori knowledge of system dynamics [34:4].

*4.1.1 Linear Systems* The basic equations for a linear Kalman filter involve the state dynamics, the solution to a stochastic difference equation, a measurement model, and the equations for a measurement update. Equations (37)–(46) show these relationships in standard matrix notation. The dynamics model for the system is:

$$\dot{\mathbf{x}}(t) = \mathbf{F}(t)\mathbf{x}(t) + \mathbf{B}(t)\mathbf{u}(t) + \mathbf{G}(t)\mathbf{w}(t) \quad (37)$$

with the system state vector  $\mathbf{x}(t)$ , the control input  $\mathbf{u}(t)$ , and a zero-mean white Gaussian noise  $\mathbf{w}(t)$ . This noise is assumed independent of  $\mathbf{x}(t)$  for all time, and has a strength,  $\mathbf{Q}(t)$ , given by:

$$E[\mathbf{w}(t)\mathbf{w}^T(t+\tau)] = \mathbf{Q}(t)\delta(\tau) \quad (38)$$

The filter propagation cycle between measurements is given by:

$$\hat{\mathbf{x}}(t_i^-) = \Phi(t_i, t_{i-1})\hat{\mathbf{x}}(t_{i-1}^+) + \int_{t_{i-1}}^{t_i} \Phi(t_i, \tau)\mathbf{B}(\tau)\mathbf{u}(\tau) d\tau \quad (39)$$

$$\begin{aligned} \mathbf{P}(t_i^-) &= \Phi(t_i, t_{i-1}) \mathbf{P}(t_{i-1}^+) \Phi^T(t_i, t_{i-1}) \\ &\quad + \int_{t_{i-1}}^{t_i} \Phi(t_i, \tau) \mathbf{G}(\tau) \mathbf{Q}(\tau) \mathbf{G}^T(\tau) \Phi^T(t_i, t_{i-1}) d\tau \end{aligned} \quad (40)$$

where  $\Phi(t, \tau)$  is the state transition matrix associated with  $\mathbf{F}(t)$ . The state transition matrix solves the differential equation:

$$\dot{\Phi}(t, \tau) = \mathbf{F}(t) \Phi(t, \tau) \quad (41)$$

subject to the constraint

$$\Phi(\tau, \tau) = \mathbf{I} \quad (42)$$

The discrete time measurements available to the system,  $\mathbf{z}(t_i)$ , are corrupted by zero-mean white Gaussian discrete-time noise  $\mathbf{v}(t_i)$  which has a covariance of  $\mathbf{R}(t_i)$ . The measurement noise  $\mathbf{v}(t)$  is assumed independent of  $\mathbf{x}(t)$  and  $\mathbf{w}(t)$  for all time. The measurement are related to the system state vector by:

$$\mathbf{z}(t) = \mathbf{H}(t_i) \mathbf{x}(t_i) + \mathbf{v}(t_i) \quad (43)$$

The measurement update cycle for the filter is:

$$\mathbf{K}(t_i) = \mathbf{P}(t_i^-) \mathbf{H}^T(t_i) [\mathbf{H}(t_i) \mathbf{P}(t_i^-) \mathbf{H}^T(t_i) + \mathbf{R}(t_i)]^{-1} \quad (44)$$

$$\hat{\mathbf{x}}(t_i^+) = \hat{\mathbf{x}}(t_i^-) + \mathbf{K}(t_i) [\mathbf{z}(t_i) - \mathbf{H}(t_i) \hat{\mathbf{x}}(t_i^-)] \quad (45)$$

$$\mathbf{P}(t_i^+) = \mathbf{P}(t_i^-) - \mathbf{K}(t_i) \mathbf{H}(t_i) \mathbf{P}(t_i^-) \quad (46)$$

In the Kalman filter equations,  $\hat{\mathbf{x}}$  represents the filter's best estimate of the actual system state  $\mathbf{x}$ ,  $\mathbf{P}$  represents the state error covariance matrix, and the vector  $\mathbf{z}$  represents measurements available to the filter. The time argument  $t_i^-$  represents the instant before incorporating a measurement,  $t_i^+$  the instant after using a measurement to update the system. For a constant  $\mathbf{F}$  matrix, the state transition matrix  $\Phi$  is given by:

$$\begin{aligned} \Phi(t_i, t_{i-1}) &= e^{\mathbf{F}(t_i - t_{i-1})} \\ &= \mathcal{L}^{-1} \left\{ [s\mathbf{I} - \mathbf{F}]^{-1} \right\} \Big|_{t=t_i - t_{i-1}} \end{aligned} \quad (47)$$

**4.1.2 Nonlinear Systems** For this aircraft tracking problem, the propagation and measurement equations used in the system model are nonlinear functions of aircraft position. This makes it necessary to use an extended Kalman filter. The dynamics model for this formulation is:

$$\dot{\mathbf{x}}(t) = \mathbf{f}[\mathbf{x}(t), \mathbf{u}(t), t] + \mathbf{G}(t)\mathbf{w}(t) \quad (48)$$

The propagation equations for this system are:

$$\hat{\mathbf{x}}(t_i^-) = \hat{\mathbf{x}}(t_{i-1}^+) + \int_{t_{i-1}}^{t_i} \mathbf{f}[\hat{\mathbf{x}}(\tau), \mathbf{u}(\tau), \tau] d\tau \quad (49)$$

$$\begin{aligned} \mathbf{P}(t_i^+) &= \Phi[t_i, t_{i-1}; \hat{\mathbf{x}}(\tau)] \mathbf{P}(t_{i-1}) \Phi^T[t_i, t_{i-1}; \hat{\mathbf{x}}(\tau)] \\ &\quad + \int_{t_{i-1}}^{t_i} \Phi[t_i, t_{i-1}; \hat{\mathbf{x}}(\tau)] \mathbf{G}(\tau) \mathbf{Q}(\tau) \mathbf{G}^T(\tau) \Phi^T[t_i, t_{i-1}; \hat{\mathbf{x}}(\tau)] d\tau \end{aligned} \quad (50)$$

The function  $\Phi[t_i, t_{i-1}; \hat{\mathbf{x}}(\tau)]$  represents the solution to the differential equation:

$$\dot{\Phi}[t_i, t_{i-1}, \hat{\mathbf{x}}(\tau)] = \mathbf{F}[t; \hat{\mathbf{x}}(\tau)] \Phi[t_i, t_{i-1}, \hat{\mathbf{x}}(\tau)] \quad (51)$$

with the boundary condition:

$$\Phi[t_i, t_i, \hat{\mathbf{x}}(\tau)] = \mathbf{I} \quad (52)$$

The measurement model and update equation for the nonlinear filter are:

$$\mathbf{z}(t_i) = \mathbf{h}[\mathbf{x}(t_i), \mathbf{u}(t_i)] + \mathbf{v}(t_i) \quad (53)$$

$$\mathbf{K}(t_i) = \mathbf{P}(t_i^-) \mathbf{H}^T[t_i; \hat{\mathbf{x}}(t_i^-)] \left\{ \mathbf{H}[t_i; \hat{\mathbf{x}}(t_i^-)] \mathbf{P}(t_i^-) \mathbf{H}^T[t_i; \hat{\mathbf{x}}(t_i^-)] + \mathbf{R}(t_i) \right\}^{-1} \quad (54)$$

$$\hat{\mathbf{x}}(t_i^+) = \hat{\mathbf{x}}(t_i^-) + \mathbf{K}(t_i) \{ \mathbf{z}(t_i) - \mathbf{h}[\hat{\mathbf{x}}(t_i^-), t_i] \} \quad (55)$$

$$\mathbf{P}(t_i^+) = \mathbf{P}(t_i^-) - \mathbf{K}(t_i) \mathbf{H}[t_i; \hat{\mathbf{x}}(t_i^-)] \mathbf{P}(t_i^-) \quad (56)$$

The extended Kalman filter recalculates the elements of the  $\mathbf{F}$  and  $\mathbf{H}$  matrices during each update and propagation cycle by evaluating partial derivatives of the

vector functions  $\mathbf{f}$  and  $\mathbf{h}$ :

$$\mathbf{F}[t; \hat{\mathbf{x}}(t)] = \left. \frac{\partial \mathbf{f}(\mathbf{x}, t)}{\partial \mathbf{x}} \right|_{\mathbf{x}=\hat{\mathbf{x}}(t_i^-)} \quad (57)$$

$$\mathbf{H}[t_i; \hat{\mathbf{x}}(t)] = \left. \frac{\partial \mathbf{h}(\mathbf{x}, t)}{\partial \mathbf{x}} \right|_{\mathbf{x}=\hat{\mathbf{x}}(t_i^-)} \quad (58)$$

When applying an extended Kalman filter to a real-time application, the requirement to recalculate  $\mathbf{F}$  and  $\mathbf{H}$  continually can impose a severe computational burden. This nonlinear formulation also makes it impossible to precompute the Kalman gains and covariance matrices ( $\mathbf{K}$  and  $\mathbf{P}$ ), a technique often used to reduce filter processing time for linear Kalman filters. Since this project involves post-flight data processing, the time required to calculate these values does not present a major problem.

The nonlinear extended Kalman filter requires the matrix  $\mathbf{F}$ , which consists of the partial derivatives of Equation (26) with respect to each state variable evaluated at the current state.

$$\mathbf{F}[t; \hat{\mathbf{x}}(t)] = \left. \frac{\partial \mathbf{f}[\mathbf{x}, t]}{\partial \mathbf{x}} \right|_{\mathbf{x}=\hat{\mathbf{x}}(t)}$$

$$\begin{aligned}
\mathbf{F}[t; \hat{\mathbf{x}}(t)] = & \left[ \begin{array}{cccccccccccccc}
0 & 0 & 0 & 1 & 0 & 0 & 0 & 0 & 0 & 0 & 0 & 0 & 0 & 0 & 0 & 0 \\
0 & 0 & 0 & 0 & 1 & 0 & 0 & 0 & 0 & 0 & 0 & 0 & 0 & 0 & 0 & 0 \\
0 & 0 & 0 & 0 & 0 & 1 & 0 & 0 & 0 & 0 & 0 & 0 & 0 & 0 & 0 & 0 \\
0 & 0 & 0 & 0 & 0 & 0 & 1 & 0 & 0 & 0 & 0 & 0 & 0 & 0 & 0 & 0 \\
0 & 0 & 0 & 0 & 0 & 0 & 0 & 1 & 0 & 0 & 0 & 0 & 0 & 0 & 0 & 0 \\
0 & 0 & 0 & 0 & 0 & 0 & 0 & 0 & 1 & 0 & 0 & 0 & 0 & 0 & 0 & 0 \\
0 & 0 & 0 & 0 & 0 & 0 & 0 & 0 & 0 & 1 & 0 & 0 & 0 & 0 & 0 & 0 \\
0 & 0 & 0 & 0 & 0 & 0 & 0 & 0 & 0 & 0 & \tau & 0 & 0 & 0 & 0 & 0 \\
0 & 0 & 0 & 0 & 0 & 0 & 0 & 0 & 0 & 0 & 0 & \tau & 0 & 0 & 0 & 0 \\
N_x & N_y & N_z & 0 & 0 & 0 & 0 & 0 & 0 & 0 & 0 & \alpha & 0 & 0 & 0 & 0 \\
0 & 0 & 0 & 0 & 0 & 0 & 0 & 0 & 0 & 0 & 0 & 0 & 0 & 0 & 0 & 0 \\
0 & 0 & 0 & 0 & 0 & 0 & 0 & 0 & 0 & 0 & 0 & 0 & 0 & 0 & 0 & 0 \\
0 & 0 & 0 & 0 & 0 & 0 & 0 & 0 & 0 & 0 & 0 & 0 & 0 & 0 & 0 & 0 \\
0 & 0 & 0 & 0 & 0 & 0 & 0 & 0 & 0 & 0 & 0 & 0 & 0 & 0 & 0 & 0 \\
0 & 0 & 0 & 0 & 0 & 0 & 0 & 0 & 0 & 0 & 0 & 0 & 0 & 0 & 0 & 0 \\
0 & 0 & 0 & 0 & 0 & 0 & 0 & 0 & 0 & 0 & 0 & 0 & 0 & 0 & 0 & 0 \\
0 & 0 & 0 & 0 & 0 & 0 & 0 & 0 & 0 & 0 & 0 & 0 & 0 & 0 & 0 & 0
\end{array} \right] \quad (59)
\end{aligned}$$

the three terms  $N_x$ ,  $N_y$  and  $N_z$  in the tenth row of the  $\mathbf{F}$  matrix in Equation (59) are given by:

$$N_x = \frac{1}{T} \frac{\partial h}{\partial P_x} \Big|_{P_x, P_y, P_z} \quad (60)$$

$$N_y = \frac{1}{T} \frac{\partial h}{\partial P_y} \Big|_{P_x, P_y, P_z} \quad (61)$$

$$N_z = \frac{1}{T} \frac{\partial h}{\partial P_z} \Big|_{P_x, P_y, P_z} \quad (62)$$

$N_x$ ,  $N_y$ , and  $N_z$  are the partial derivatives of altitude with respect to  $P_x$ ,  $P_y$ , and  $P_z$  evaluated at the current aircraft position. Calculating  $\mathbf{F}$  with these partial derivatives gives the form for an extended Kalman filter. The equation for aircraft altitude given position is:

$$h = \frac{P_z}{\sin L} - \frac{a(1 - \epsilon^2)}{\sqrt{1 - \epsilon^2 \sin^2 L}} \quad (63)$$

This equation for altitude requires the aircraft geodetic latitude,  $L$ . The geodetic latitude,  $L_c$ , is not equal to the geocentric latitude. The geodetic latitude is given by the trigonometric relationship

$$L_c = \arcsin \frac{P_z}{\sqrt{P_x^2 + P_y^2 + P_z^2}} \quad (64)$$

Geodetic latitude  $L$  is related to geocentric latitude  $L_c$  using the relationship

$$L = L_c + f \sin(2L) \quad (65)$$

where  $f$  is the flattening ratio, or ellipticity, based on the semi-major and semi-minor axes of the ellipsoid [4]. This equation cannot be solved for  $L$  in closed form given  $L_c$ , but it can be expanded into a sequence, successively evaluating the right side of the equation as a new estimate for  $L$ . When treating the equation for  $L$  iteratively, the value quickly converges to within 0.001 degrees of the proper answer. Unfortunately, convergence to the exact value is slow. An approximation is made by including three terms of this sequence.

$$L \approx L_c + f \sin\{2[L_c + f \sin(2L_c)]\} \quad (66)$$

Knowing the relationship between  $L$  and the position vector allows computation of the partial derivatives with respect to geodetic latitude:

$$\begin{aligned} N_x &= \left. \frac{\partial h}{\partial P_x} \right|_{P_x, P_y, P_z} \\ &= \left. \frac{\partial h}{\partial L} \frac{\partial L}{\partial P_x} \right|_{P_x, P_y, P_z} \\ &= \left. \frac{\partial}{\partial P_x} \left[ \frac{P_z}{\sin L} - \frac{a(1-\epsilon^2)}{\sqrt{1-\epsilon^2 \sin^2 L}} \right] \frac{\partial L}{\partial P_x} \right|_{P_x, P_y, P_z} \\ &= \left[ \frac{-P_z \cos L}{\sin^2 L} - \frac{a(1-\epsilon^2)\epsilon^2 \sin L \cos L}{(1-\epsilon^2 \sin^2 L)^{\frac{3}{2}}} \right] \left. \frac{\partial L}{\partial P_x} \right|_{P_x, P_y, P_z} \end{aligned} \quad (67)$$

$$N_y = \left[ \frac{-P_z \cos L}{\sin^2 L} - \frac{a(1-\epsilon^2)\epsilon^2 \sin L \cos L}{(1-\epsilon^2 \sin^2 L)^{\frac{3}{2}}} \right] \left. \frac{\partial L}{\partial P_y} \right|_{P_x, P_y, P_z} \quad (68)$$

$$N_z = \left\{ \frac{1}{\sin L} - \left[ \frac{P_z \cos L}{\sin^2 L} + \frac{a(1-\epsilon^2)\epsilon^2 \sin L \cos L}{(1-\epsilon^2 \sin^2 L)^{\frac{3}{2}}} \right] \left. \frac{\partial L}{\partial P_z} \right\} \right|_{P_x, P_y, P_z} \quad (69)$$

The partial derivatives of  $L$  can be taken with respect to the geocentric latitude using the relationship between  $L_c$  and  $L$  derived in Equation (66):

$$\begin{aligned}\frac{\partial L}{\partial P_x} &= \frac{\partial L}{\partial L_c} \frac{\partial L_c}{\partial P_x} \\ &= \frac{\partial}{\partial L_c} [L_c + f \sin\{2[L_c + f \sin(2L_c)]\}] \frac{\partial L_c}{\partial P_x} \\ &= [1 + 2f \cos\{2L_c + 2f \sin(2L_c)\}] \\ &\quad + [4f^2 \cos(2L_c) \cos\{2L_c + 2f \sin(2L_c)\}] \frac{\partial L_c}{\partial P_x}\end{aligned}\quad (70)$$

$$\begin{aligned}\frac{\partial L}{\partial P_y} &= [1 + 2f \cos\{2L_c + 2f \sin(2L_c)\}] \\ &\quad + [4f^2 \cos(2L_c) \cos\{2L_c + 2f \sin(2L_c)\}] \frac{\partial L_c}{\partial P_y}\end{aligned}\quad (71)$$

$$\begin{aligned}\frac{\partial L}{\partial P_z} &= [1 + 2f \cos\{2L_c + 2f \sin(2L_c)\}] \\ &\quad + [4f^2 \cos(2L_c) \cos\{2L_c + 2f \sin(2L_c)\}] \frac{\partial L_c}{\partial P_z}\end{aligned}\quad (72)$$

Finally, the partial derivatives of geocentric latitude,  $L_c$ , with respect to  $P_x$ ,  $P_y$ , and  $P_z$  are given by:

$$\begin{aligned}\frac{\partial L_c}{\partial P_x} &= \frac{\partial}{\partial P_x} \left[ \arcsin \left( \frac{P_z}{\sqrt{P_x^2 + P_y^2 + P_z^2}} \right) \right] \\ &= \frac{-P_x P_z}{(P_x^2 + P_y^2 + P_z^2) \sqrt{P_x^2 + P_y^2}}\end{aligned}\quad (73)$$

$$\frac{\partial L_c}{\partial P_y} = \frac{-P_y P_z}{(P_x^2 + P_y^2 + P_z^2) \sqrt{P_x^2 + P_y^2}}\quad (74)$$

$$\frac{\partial L_c}{\partial P_z} = \frac{\sqrt{P_x^2 + P_y^2}}{P_x^2 + P_y^2 + P_z^2}\quad (75)$$

Substituting Equations (73) through (75) into the partial derivatives of geodetic latitude, Equations (70) through (72), and substituting those results into the equations for  $N_x$ ,  $N_y$  and  $N_z$  gives the required partial derivatives to fill the  $\mathbf{F}$  matrix.

Since the measurement model involves nonlinear functions of state variables, the filter again uses partial derivatives to calculate matrix elements for  $\mathbf{H}$ . The

required range partials correspond to unit line of site vectors and are given by:

$$\begin{aligned}\frac{\partial R}{\partial x} &= \frac{\partial}{\partial x} \left[ \sqrt{(P_x - X_B)^2 + (P_y - Y_B)^2 + (P_z - Z_B)^2} \right] \\ &= \frac{P_x - X_B}{\sqrt{(P_x - X_B)^2 + (P_y - Y_B)^2 + (P_z - Z_B)^2}}\end{aligned}\quad (76)$$

$$\frac{\partial R}{\partial y} = \frac{P_y - Y_B}{\sqrt{(P_x - X_B)^2 + (P_y - Y_B)^2 + (P_z - Z_B)^2}} \quad (77)$$

$$\frac{\partial R}{\partial z} = \frac{P_z - Z_B}{\sqrt{(P_x - X_B)^2 + (P_y - Y_B)^2 + (P_z - Z_B)^2}} \quad (78)$$

Knowing the north and east components of the vector from the beacon to the aircraft, represented by  $N$  and  $E$ , along with the magnetic variation (var) at the beacon site, allows calculation of the partial derivatives of bearing with respect to aircraft position:

$$\begin{aligned}\frac{\partial B}{\partial x} &= \frac{\partial}{\partial x} \left( \tan^{-1} \frac{E}{N} + \text{var} \right) \\ &= \left( \frac{N^2}{N^2 + E^2} \right) \frac{\partial}{\partial x} \left( \frac{E}{N} \right) \\ &= \frac{1}{N^2 + E^2} \left( N \frac{\partial E}{\partial x} - E \frac{\partial N}{\partial x} \right)\end{aligned}\quad (79)$$

$$\frac{\partial B}{\partial y} = \frac{1}{N^2 + E^2} \left( N \frac{\partial E}{\partial y} - E \frac{\partial N}{\partial y} \right) \quad (80)$$

$$\frac{\partial B}{\partial z} = \frac{1}{N^2 + E^2} \left( N \frac{\partial E}{\partial z} - E \frac{\partial N}{\partial z} \right) \quad (81)$$

Substituting the partial derivatives given below into Equations (79) through (81) allows for complete evaluation of the terms required in the filter:

$$\begin{aligned}\frac{\partial E}{\partial x} &= \frac{\partial}{\partial x} \left\{ -\sin l_B (P_x - X_B) + \cos l_B (P_y - Y_B) \right\} \\ &= -\sin l_B\end{aligned}\quad (82)$$

$$\frac{\partial E}{\partial y} = \cos l_B \quad (83)$$

$$\frac{\partial E}{\partial z} = 0 \quad (84)$$

$$\frac{\partial N}{\partial x} = \frac{\partial}{\partial x} \left\{ -\sin L_B \cos l_B (P_x - X_B) \right.$$

$$\begin{aligned} & - \sin L_B \sin l_B (P_y - Y_B) + \cos L_B (P_z - Z_B) \} \\ = & - \sin L_B \cos l_B \end{aligned} \tag{85}$$

$$\frac{\partial N}{\partial y} = - \sin L_B \sin l_B \tag{86}$$

$$\frac{\partial N}{\partial z} = \cos L_B \tag{87}$$

#### 4.2 System Propagation

The operation of a Kalman filter normally separates into two processes. Between incorporating measurements, the filter propagates the last estimate of the system state toward the next measurement time. It propagates forward in time for a standard filter, and both forward and backward in time for an optimal smoother, which is covered later in this chapter. Since the system model considered here has no commanded inputs, the term  $u(t)$  becomes zero in the general filter equations.

Although the matrix  $\mathbf{F}$  varies with time, the changes occur slowly. This behavior was approximated by treating  $\mathbf{F}$  as piecewise constant over the 0.5 sec sample periods. The state transition matrix to propagate the system states forward in time,  $\Phi$ , is given by:

$$\Phi(t_{i-1}, t_i) = \mathcal{L}^{-1} \{ [s\mathbf{I} - \mathbf{F}]^{-1} \} \tag{88}$$

$$= \mathcal{L}^{-1} \left\{ \begin{bmatrix} s & 0 & 0 & -1 & 0 & 0 & 0 & 0 & 0 & 0 & 0 & 0 \\ 0 & s & 0 & 0 & -1 & 0 & 0 & 0 & 0 & 0 & 0 & 0 \\ 0 & 0 & s & 0 & 0 & -1 & 0 & 0 & 0 & 0 & 0 & 0 \\ 0 & 0 & 0 & s & 0 & 0 & -1 & 0 & 0 & 0 & 0 & 0 \\ 0 & 0 & 0 & 0 & s & 0 & 0 & -1 & 0 & 0 & 0 & 0 \\ 0 & 0 & 0 & 0 & 0 & s & 0 & 0 & -1 & 0 & 0 & 0 \\ 0 & 0 & 0 & 0 & 0 & 0 & s - \tau & 0 & 0 & 0 & 0 & 0 \\ 0 & 0 & 0 & 0 & 0 & 0 & 0 & s - \tau & 0 & 0 & 0 & 0 \\ 0 & 0 & 0 & 0 & 0 & 0 & 0 & 0 & s - \tau & 0 & 0 & 0 \\ -N_x & -N_y & -N_z & 0 & 0 & 0 & 0 & 0 & 0 & s - \alpha & 0 & 0 \\ 0 & 0 & 0 & 0 & 0 & 0 & 0 & 0 & 0 & 0 & s & 0 \\ 0 & 0 & 0 & 0 & 0 & 0 & 0 & 0 & 0 & 0 & 0 & s \\ 0 & 0 & 0 & 0 & 0 & 0 & 0 & 0 & 0 & 0 & 0 & 0 \\ 0 & 0 & 0 & 0 & 0 & 0 & 0 & 0 & 0 & 0 & 0 & s \\ 0 & 0 & 0 & 0 & 0 & 0 & 0 & 0 & 0 & 0 & 0 & 0 \\ 0 & 0 & 0 & 0 & 0 & 0 & 0 & 0 & 0 & 0 & 0 & s \end{bmatrix}^{-1} \right\} \quad (89)$$

The computer program MACSYMA [54] provided the inverse of this matrix:

$$= \mathcal{L}^{-1} \left\{ \begin{bmatrix} \frac{1}{s} & 0 & 0 & \frac{1}{s^2} & 0 & 0 & \frac{1}{d_2} & 0 & 0 & 0 & 0 & 0 & 0 & 0 & 0 & 0 \\ 0 & \frac{1}{s} & 0 & 0 & \frac{1}{s^2} & 0 & 0 & \frac{1}{d_2} & 0 & 0 & 0 & 0 & 0 & 0 & 0 \\ 0 & 0 & \frac{1}{s} & 0 & 0 & \frac{1}{s^2} & 0 & 0 & \frac{1}{d_2} & 0 & 0 & 0 & 0 & 0 & 0 \\ 0 & 0 & 0 & \frac{1}{s} & 0 & 0 & \frac{1}{d_1} & 0 & 0 & 0 & 0 & 0 & 0 & 0 & 0 \\ 0 & 0 & 0 & 0 & \frac{1}{s} & 0 & 0 & \frac{1}{d_1} & 0 & 0 & 0 & 0 & 0 & 0 & 0 \\ 0 & 0 & 0 & 0 & 0 & \frac{1}{s} & 0 & 0 & \frac{1}{d_1} & 0 & 0 & 0 & 0 & 0 & 0 \\ 0 & 0 & 0 & 0 & 0 & 0 & \frac{1}{s} & 0 & 0 & \frac{1}{d_1} & 0 & 0 & 0 & 0 & 0 \\ 0 & 0 & 0 & 0 & 0 & 0 & 0 & \frac{1}{d_3} & 0 & 0 & 0 & 0 & 0 & 0 & 0 \\ 0 & 0 & 0 & 0 & 0 & 0 & 0 & 0 & \frac{1}{d_3} & 0 & 0 & 0 & 0 & 0 & 0 \\ 0 & 0 & 0 & 0 & 0 & 0 & 0 & 0 & 0 & \frac{1}{d_3} & 0 & 0 & 0 & 0 & 0 \\ \frac{N_x}{d_5} & \frac{N_x}{d_5} & \frac{N_x}{d_5} & \frac{N_x}{d_5} & \frac{N_x}{d_5} & \frac{N_x}{d_5} & \frac{N_x}{d_7} & \frac{N_x}{d_7} & \frac{1}{d_4} & 0 & 0 & 0 & 0 & 0 & 0 \\ 0 & 0 & 0 & 0 & 0 & 0 & 0 & 0 & 0 & 0 & \frac{1}{s} & 0 & 0 & 0 & 0 \\ 0 & 0 & 0 & 0 & 0 & 0 & 0 & 0 & 0 & 0 & 0 & \frac{1}{s} & 0 & 0 & 0 \\ 0 & 0 & 0 & 0 & 0 & 0 & 0 & 0 & 0 & 0 & 0 & 0 & \frac{1}{s} & 0 & 0 \\ 0 & 0 & 0 & 0 & 0 & 0 & 0 & 0 & 0 & 0 & 0 & 0 & 0 & \frac{1}{s} & 0 \\ 0 & 0 & 0 & 0 & 0 & 0 & 0 & 0 & 0 & 0 & 0 & 0 & 0 & 0 & \frac{1}{s} \end{bmatrix} \right\}^{-1} \quad (90)$$

Table 3 lists the denominators found in the Laplace transform of the state transition matrix. These have been listed separately due to the complexity of the matrix.

Table 3. Matrix Denominator Terms

$d_1$	$s(s - \tau)$
$d_2$	$s^2(s - \tau)$
$d_3$	$s - \tau$
$d_4$	$s - \alpha$
$d_5$	$s(s - \alpha)$
$d_6$	$s^2(s - \alpha)$
$d_7$	$s^2(s - \alpha)(s - \tau)$

Table 4. Laplace Transform Pairs

$F(s)$	$f(t)$
$\frac{1}{s}$	1
$\frac{1}{s+a}$	$e^{-at}$
$\frac{1}{s^2}$	$t$
$\frac{1}{s(s+a)}$	$\frac{1}{a}(1 - e^{-at})$
$\frac{1}{s^2(s+a)}$	$\frac{1}{a^2}(at - 1 + e^{-at})$
$\frac{1}{s^2(s+a)(s+b)}$	$\frac{1}{(ab)^2}(abt - a - b) + \frac{e^{-at}}{a^2(b-a)} + \frac{e^{-bt}}{b^2(a-b)}$

Table 4 gives the required inverse Laplace transforms for this state transition matrix.

#### 4.3 System Updates

After propagating a best estimate of the current state vector,  $\hat{\mathbf{x}}(t_i^-)$ , and the covariance describing the uncertainty of that value,  $\mathbf{P}(t_i^-)$ , the filter incorporates available measurements to improve the accuracy of those estimated values. The Kalman gain,  $\mathbf{K}(t_i)$ , tells the filter how much confidence to place in the new measurements, relative to the output of the propagation cycle. For extreme Kalman gains, the filter may totally ignore its own propagated state estimate and place full confidence in the measurements, or the filter can completely ignore the measurements if it does not consider the new data accurate enough. The equations used

to perform a measurement update with an extended Kalman filter are given by Equations (54) to (56).

#### 4.4 Optimal Smoothing

The Kalman filter equations outlined above provide the optimal estimate of the system state based upon all measurements up to and including the one at time  $t_i$ . An optimal smoother extends that idea to include all available measurements, including measurements taken in the future. This non-causal nature limits optimal smoothing to post-flight processing, but by providing additional information to the estimator, it can usually provide better position estimates than a filter.

**4.4.1 Backward Filter** The optimal smoother uses two separate Kalman filters. The forward running filter uses the equations from the preceding section. The second filter starts at the final time and runs backward toward the initial time. By combining information in the forward filter, incorporating all measurements from  $t_{\text{initial}}$  to  $t_i$ , and the information in the backward filter, which uses measurements  $t_{i+1}$  to  $t_{\text{final}}$ , the smoother can use all the measurements to estimate the system state.

The backward filter normally runs in an inverse covariance form [35:6]. In this form, it is easier to work with a state vector  $\hat{\mathbf{y}}_b$  that represents the product of the backward inverse covariance,  $\mathbf{P}_b^{-1}$ , and the backward filter state,  $\hat{\mathbf{x}}_b$ . These values are initialized with:

$$\hat{\mathbf{y}}_b(t_{\text{final}}^-) = \mathbf{0} \quad (91)$$

$$\mathbf{P}_b^{-1}(t_{\text{final}}^-) = \mathbf{0} \quad (92)$$

For each measurement, taken at time  $t_i$ , the backward filter is updated using:

$$\hat{\mathbf{y}}_b(t_i^+) = \hat{\mathbf{y}}_b(t_i^-) + \mathbf{H}^T(t_i)\mathbf{R}^{-1}(t_i)\mathbf{z}(t_i) \quad (93)$$

$$\mathbf{P}_b^{-1}(t_i^+) = \mathbf{P}_b^{-1}(t_i^-) + \mathbf{H}^T(t_i)\mathbf{R}^{-1}(t_i)\mathbf{H}(t_i) \quad (94)$$

In the backward filter,  $t_i^-$  represents the instant before the back filter receives the measurement, just as in the forward filter. However, in the backward filter,  $t_i^-$  is closer to  $t_{\text{final}}$  than  $t_{\text{initial}}$ , and  $t_i^+$  represents the instant after the measurement is incorporated, which is further from  $t_{\text{final}}$  than from  $t_{\text{initial}}$ .

Assuming no commanded inputs, the backward filter propagates to the next time using:

$$\mathbf{J}(t_i) = \mathbf{P}_b^{-1}(t_i^+) \mathbf{G}_d(t_{i-1}) [\mathbf{G}_d^T(t_{i-1}) \mathbf{P}_b^{-1}(t_i^+) \mathbf{G}_d(t_{i-1}) + \mathbf{Q}_d^{-1}(t_{i-1})]^{-1} \quad (95)$$

$$\mathbf{L}(t_i) = \mathbf{I} - \mathbf{J}(t_i) \mathbf{G}_d^T(t_{i-1}) \quad (96)$$

$$\mathbf{M}(t_i) = \mathbf{L}(t_i) \mathbf{P}_b^{-1}(t_i^+) \mathbf{L}^T(t_i) + \mathbf{J}(t_i) \mathbf{Q}_d^{-1}(t_{i-1}) \mathbf{J}^T(t_i) \quad (97)$$

$$\hat{\mathbf{y}}_b(t_i^-) = \Phi^T(t_i, t_{i-1}) \mathbf{L}(t_i) \hat{\mathbf{y}}_b(t_i^+) \quad (98)$$

$$\mathbf{P}_b^{-1}(t_{i-1}) = \Phi^T(t_i, t_{i-1}) \mathbf{M}(t_i) \Phi(t_i, t_{i-1}) \quad (99)$$

In the preceding equations,  $\mathbf{G}_d$  is the identity matrix, and  $\mathbf{Q}_d$  corresponds to the integral term in Equation 50:

$$\mathbf{Q}_d(t_{i-1}) = \int_{t_{i-1}}^{t_i} \Phi[t_i, t_{i-1}; \hat{\mathbf{x}}(\tau)] \mathbf{G}(\tau) \mathbf{Q}(\tau) \mathbf{G}^T(\tau) \Phi^T[t_i, t_{i-1}; \hat{\mathbf{x}}(\tau)] d\tau \quad (100)$$

**4.4.2 Combining Filter Data** The backward filter executes after the forward filter generates state and covariance estimates for the entire flight. The forward filter uses an extended Kalman filter with a nonlinear system model. This allows the backward filter to operate with a linear perturbation filter which uses the forward filter results as the nominal state values. For each measurement, the smoother calculates state estimates by combining the  $\hat{\mathbf{x}}(t_i^+)$  and  $\mathbf{P}(t_i^+)$  values from the forward filter with the  $\hat{\mathbf{y}}_b(t_i^-)$  and  $\mathbf{P}_b^{-1}(t_i^-)$  from the backward filter via:

$$\mathbf{X}(t_i) = [\mathbf{I} + \mathbf{P}(t_i^+) \mathbf{P}_b^{-1}(t_i^-)]^{-1} \quad (101)$$

$$\mathbf{W}(t_i) = \mathbf{P}(t_i^+) \mathbf{X}^T(t_i) \quad (102)$$

$$\mathbf{Y}(t_i) = \mathbf{I} - \mathbf{W}(t_i) \mathbf{P}_b^{-1}(t_i^-) \quad (103)$$

$$\mathbf{P}(t_i/t_{\text{final}}) = \mathbf{Y}(t_i) \mathbf{P}(t_i^+) \mathbf{Y}^T(t_i)$$

$$+ \mathbf{W}(t_i) \mathbf{P}_b^{-1}(t_i^-) \mathbf{W}^T(t_i) \quad (104)$$

$$\hat{\mathbf{x}}(t_i/t_{\text{final}}) = \mathbf{X}(t_i) \hat{\mathbf{x}}(t_i^+) + \mathbf{P}(t_i/t_{\text{final}}) \hat{\mathbf{y}}_b(t_i^-) \quad (105)$$

#### 4.5 Programming Environment

The programs written for this project are coded in Fortran-77 on a Digital Equipment Corporation (DEC) computer running the VMS operating system. The factors supporting this programming environment are:

- John Franzen's initial programs investigating this type of tracking for the 4950th Test Wing are written in Fortran.
- The data analysts in the 4950th Test Wing normally use Fortran for all programming. Using it for this project makes program updates and maintenance easier.
- Both AFIT and the Test Wing computers support this configuration, easing the transition from development at AFIT to use in the Wing.

#### 4.6 System Modeling

As explained in Chapter III, the model used in the Kalman smoother contains fifteen states in order to model positions, velocities and accelerations in three dimensions, the lag in the altimeter, and biases in the five measurements. Driving this system are eight independent noise sources which enter the system's acceleration and bias states directly.

*4.6.1 Filter Tuning* In the filter's model of the real world, values are assigned to the strengths of the driving noise,  $\mathbf{Q}$ , and the covariance of the measurement noise,  $\mathbf{R}$ . Table 5 shows the values chosen for the diagonal elements of the matrix  $\mathbf{Q}$ . The acceleration driving noise strengths correspond to the  $3\sigma$  value for aircraft acceleration of  $15m/s^2$ , or approximately  $1.5g's$  in any direction.

Table 5. Driving Noise Strengths

$Q_{1,1}$	$50m^2/s^5$	Accelerations
$Q_{2,2}$	$50m^2/s^5$	
$Q_{3,3}$	$50m^2/s^5$	
$Q_{4,4}$	$10^{-4}m^2/s$	TACAN 1 Range
$Q_{5,5}$	$10^{-6}rad^2/s$	TACAN 1 Bearing
$Q_{6,6}$	$10^{-4}m^2/s$	TACAN 2 Range
$Q_{7,7}$	$10^{-6}rad^2/s$	TACAN 2 Bearing
$Q_{8,8}$	$100m^2/s$	Altimeter

Table 6. Measurement Noise Variances

$R_{1,1}$	$400m^2$	Range Bias 1
$R_{2,2}$	$10^{-4}rad^2$	Bearing Bias 1
$R_{3,3}$	$400m^2$	Range Bias 2
$R_{4,4}$	$10^{-4}rad^2$	Bearing Bias 2
$R_{5,5}$	$100m^2$	Altimeter Bias

These values for the first three diagonal elements of  $\mathbf{Q}$  is based on the relationship  $Q = \sigma T/2$  [37], using the time constant  $T$  from Equation (3). Small range and altimeter bias driving noise strengths reflect the essentially constant nature of these biases while preventing the tracker from totally ignoring future measurements related to these states. These values are the result of iteratively tuning the filter until it could track a maneuvering target.

Table 6 shows the values assigned to the diagonal elements of the  $\mathbf{R}$  matrix. These values are based on statistical data collected by the 4950th Test Wing [39] and the Royal Aircraft Establishment [46].

In both the  $\mathbf{Q}$  and  $\mathbf{R}$  matrices, the off-diagonal terms are set to zero which represents statistical independence of the measurements. This assumes errors from one beacon are independent of errors from a second beacon since they are geographically isolated from each other. The range and bearing information provided by

a single TACAN are considered independent since they involve different measurement mechanisms. This same reasoning allows treating the barometrically measured altitude as independent of the ranges and bearings determined with radio signals.

## *V. Computer Simulations*

A complete evaluation of the tracking technique developed in this thesis requires TACAN and altimeter measurements collected while a high-precision reference system tracks the aircraft. Funding and scheduling considerations have prevented the Test Wing from providing this type of data. Simulated measurement data based on estimates of real-world noise characteristics provide the basis for this chapter.

### *5.1 Measurement Data Generation*

Input data to the dual TACAN tracker is generated using a combination of five computer programs. Aircraft maneuver commands are entered into PROFGEN, an aircraft flight profile generating program developed by Stan Musick at the Air Force Wright Aeronautical Laboratories [40]. This program uses a high-order numerical integrator to solve the aircraft equations of motion and provides realistic values for aircraft position, velocity and acceleration.

The output of PROFGEN is combined with a list of TACAN beacons used during the flight and the TACAN positions. The resulting file contains the true ranges and bearings from the beacons to the aircraft. Finally, the measurement file is corrupted by noise, with each TACAN beacon having its own noise statistics assigned to representative values [39,46]. Table 7 outlines the steps necessary to create a simulated measurement file.

### *5.2 Test Scenario*

The measurement file simulates a 15-minute test flight starting from a stationary position on the runway at Wright-Patterson AFB. At time zero, the plane accelerates and takes off to the southwest. After climbing to an altitude of 1600 meters, the plane executes a slow turn to the left. As the flight progresses, the

Table 7. Creating Simulation Data

Input Data	Program	Output Data
Maneuver Commands	PROFGEN	Aircraft Position
Aircraft Position TACAN Positions	INSTRM	Noise Free Altimeter and TACAN Measurements
Noise Free Measurements	CORRUPT	Noise Corrupted Measurements

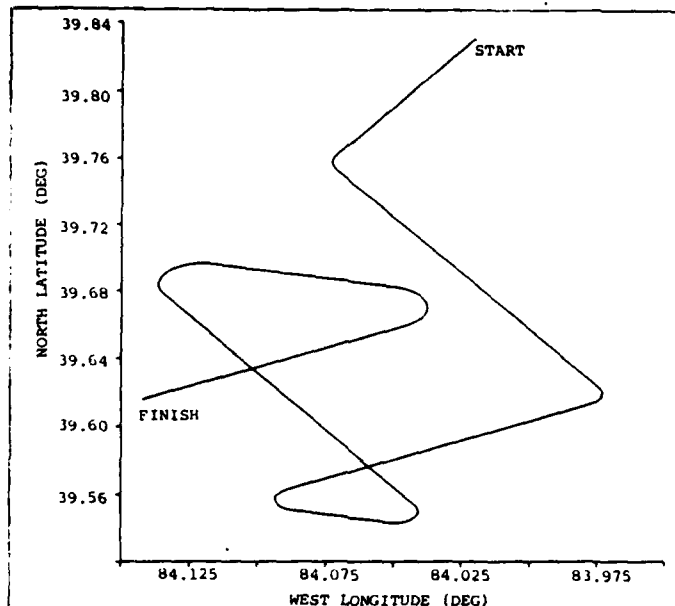


Figure 7. Test Flight Ground Track

plane also performs a slow turn to the right and four high-speed turns. The sample flight includes several velocity and altitude changes. These maneuvers represent the type of flying usually involved in flight tests conducted by the 4950th Test Wing. Figure 7 gives a map-like view of this flight path, with the aircraft travelling from the upper right to the lower left of the plot.

Figures 8 and 9 show the aircraft altitude and velocity plotted as functions of time. Both graphs begin with the aircraft stationary on the runway at time  $t = -40$  seconds. The aircraft begins the take-off acceleration at  $t = 0$  and takes off at  $t = 15$  seconds.

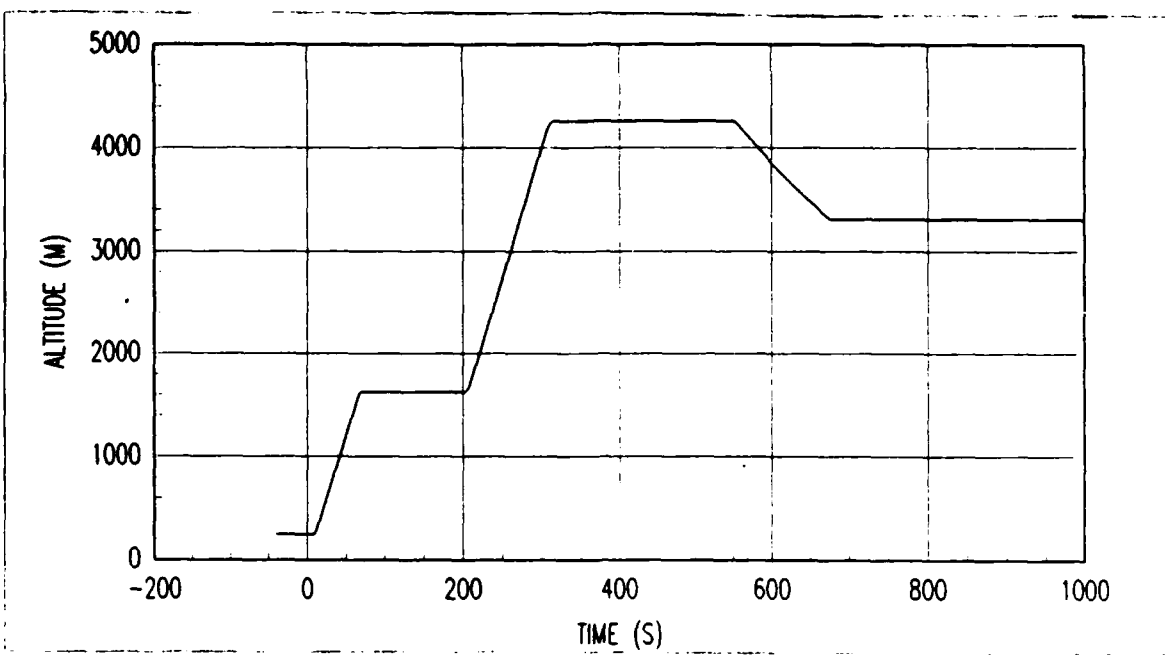


Figure 8. Test Flight Altitude History

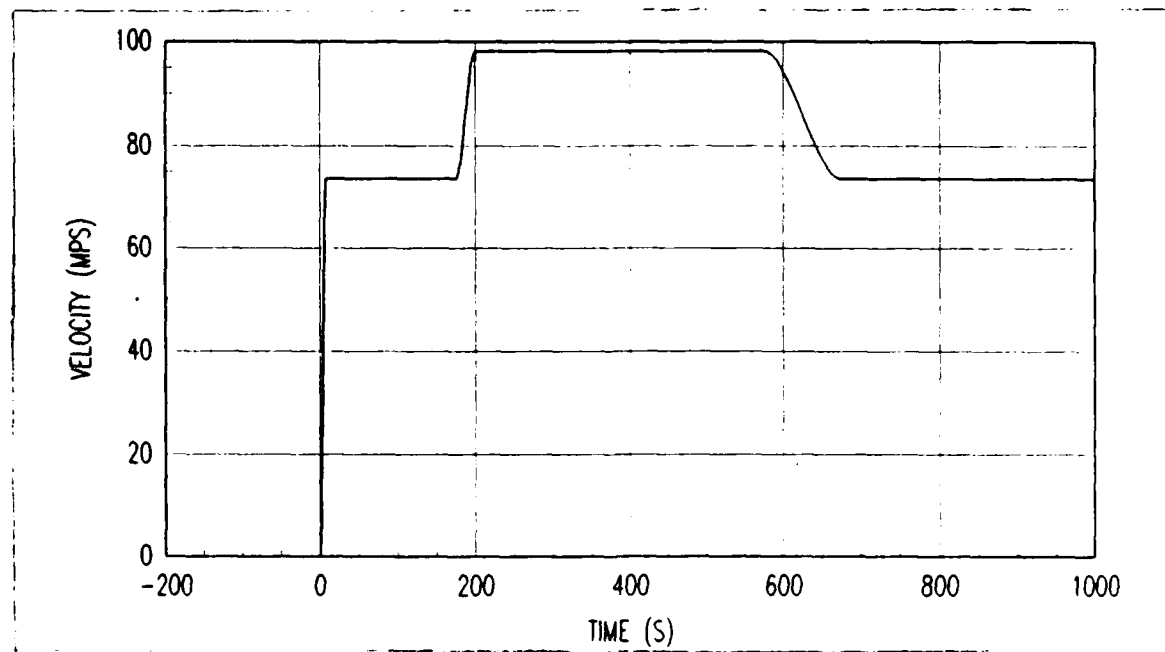


Figure 9. Test Flight Velocity History

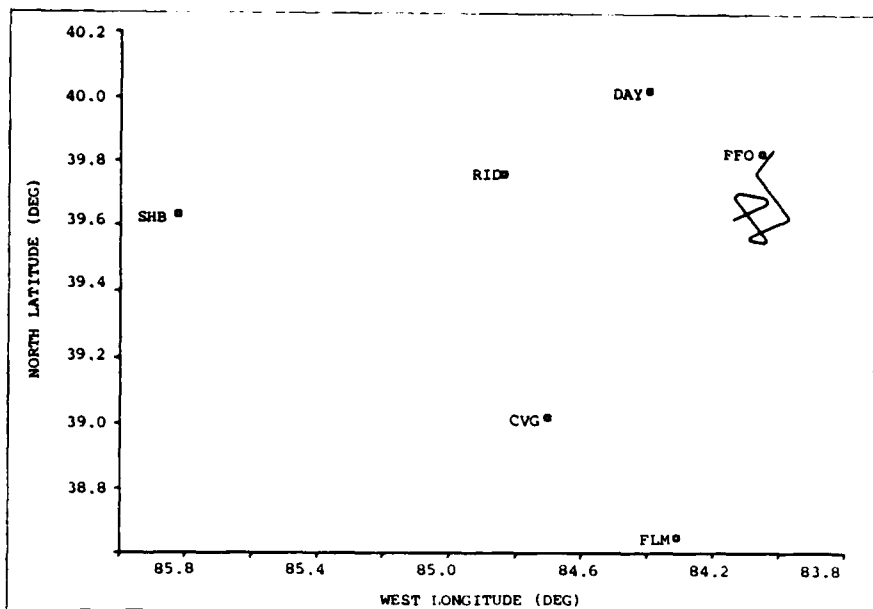


Figure 10. TACAN Beacon Locations

An important operation for the tracker involves adjusting to constantly varying measurement sources as different pairs of TACAN beacons provide measurements during a flight. This test scenario uses six different beacons, retuning the on-board transceivers at times  $t = -10$ ,  $t = 45$ ,  $t = 200$ , and  $t = 500$  seconds. Figure 10 shows the position of the aircraft track in relation to the ground beacons.

The second reason for changing beacons throughout the flight involves the uncertainty involved when resolving multiple range measurements. The minimum uncertainty occurs when the difference in bearings from the aircraft to the two TACAN beacons, or cut angle, equals 90 degrees [39:F3]. TACAN selection should maintain this cut angle between 60 and 120 degrees for best tracker performance. During this test flight, the angle between the TACANs varies from 40 to 85 degrees.

### 5.3 System Performance

*5.3.1 Single Simulation Performance* The Kalman smoother performance is evaluated by comparing smoother output, expressed in earth-centered, earth-fixed coordinates with the original, noise-free values derived from PROFGEN.

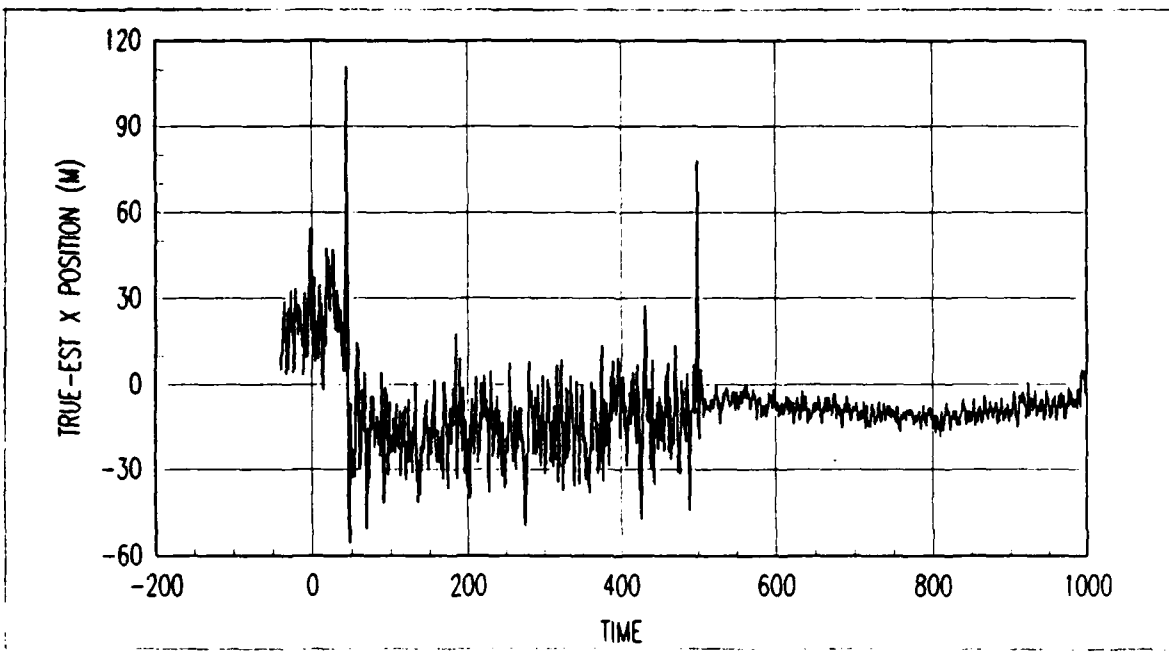


Figure 11. Example of X Position Error

Figure 11 shows the component of the position error in the  $x$  direction, which is calculated by subtracting the tracker value for  $\hat{P}_x$  from the true value  $P_x$ . This graph has a temporally averaged mean error of  $-9$  meters and a temporally derived standard deviation of  $14$  meters.

This same technique was used to generate the error plots in the  $y$  and  $z$  directions shown in Figures 12 and 13. The  $y$  error component has a temporally averaged mean value of  $15$  meters and a temporal standard deviation of  $22$  meters. The  $z$  component of error has a temporally averaged mean value of  $42$  meters and a temporal standard deviation of  $21$  meters.

Radial error provides another means to assess tracker accuracy. This is the method of evaluating navigation accuracy outlined in the North Atlantic Treaty Organization (NATO) Standardization Agreement (STANAG) 4278, "Method of Expressing Navigation Accuracy" [5]. The radial error distance ( $R_e$ ) is computed using the true position  $(x_t, y_t, z_t)$  and the smoother estimate of position  $(\hat{P}_x, \hat{P}_y, \hat{P}_z)$ .

$$R_e = \sqrt{(x_t - \hat{P}_x)^2 + (y_t - \hat{P}_y)^2 + (z_t - \hat{P}_z)^2} \quad (106)$$

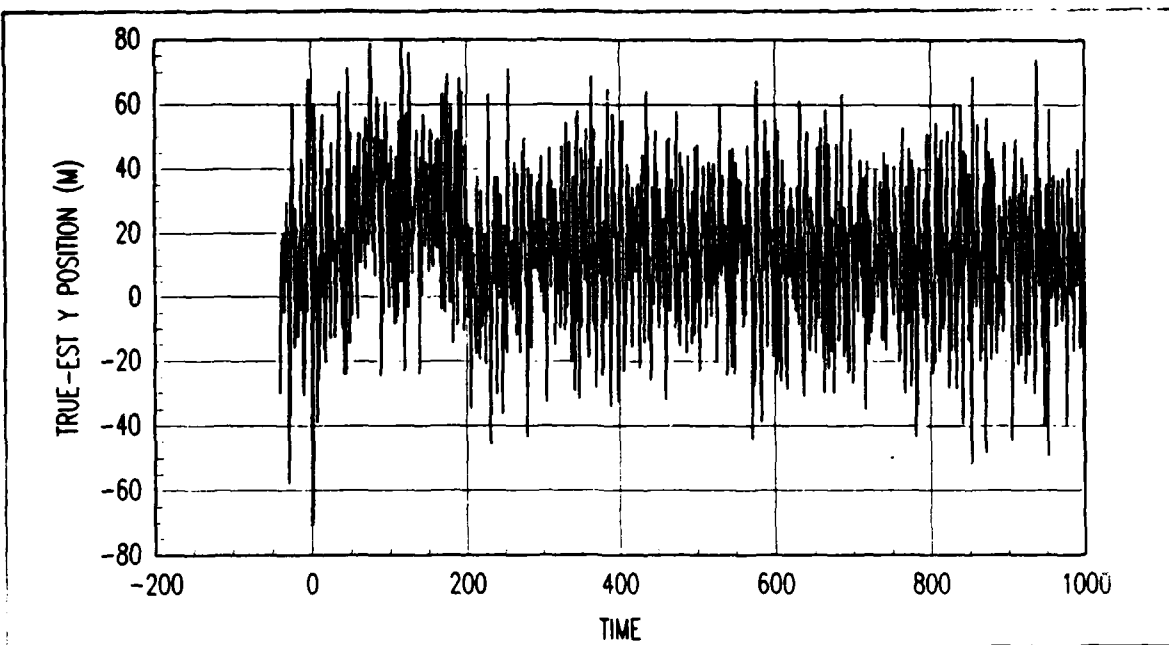


Figure 12. Example of Y Position Error

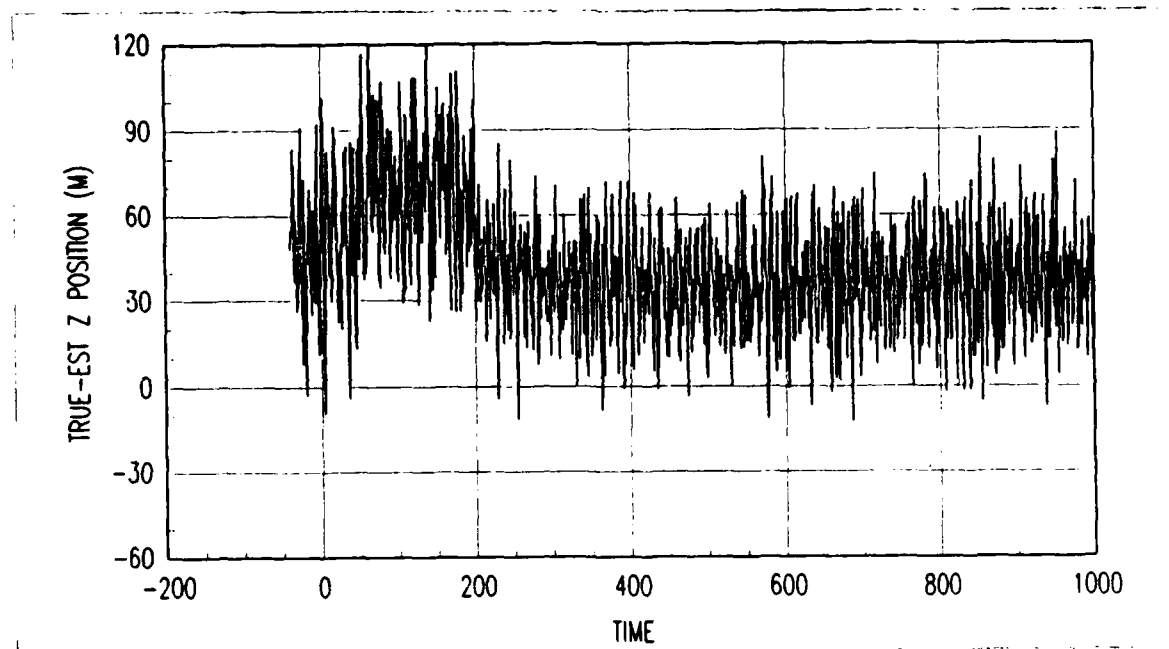


Figure 13. Example of Z Position Error

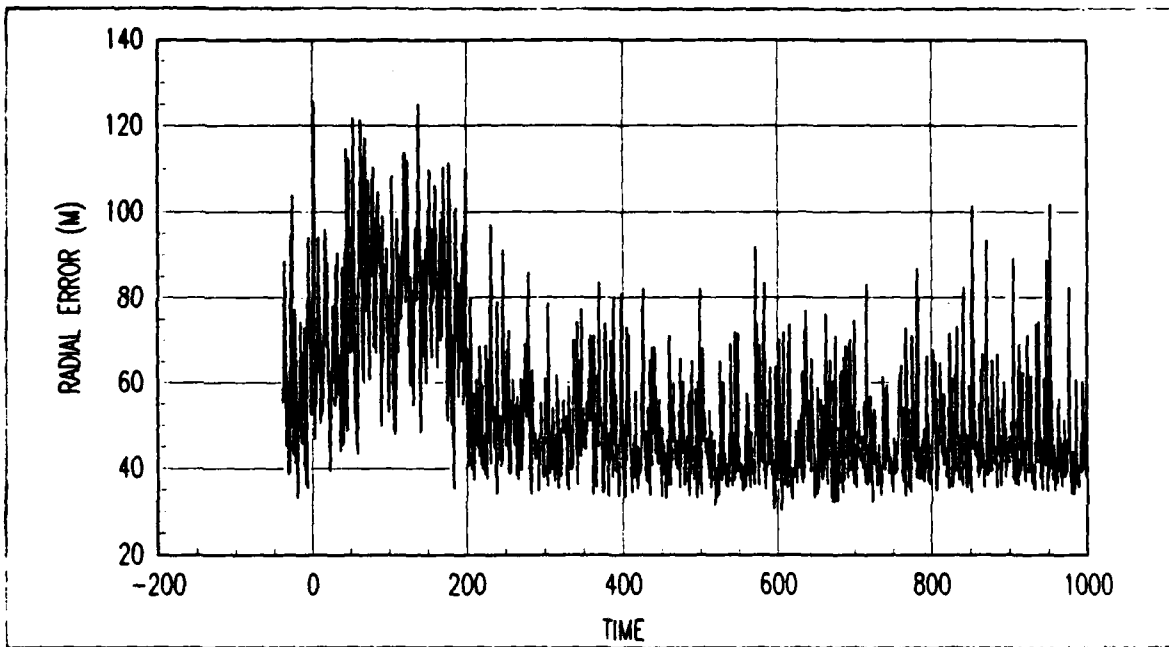


Figure 14. Example of Radial Error

Figure 14 shows the radial error for one simulation run plotted versus time. The shift in the error plot at time  $t = 200$  seconds corresponds to a change in TACAN beacons used by the system. The opportunity to recalculate measurement biases and more favorable solution geometry allows the filter to estimate the aircraft position more accurately.

According to STANAG 4278, a positioning system should have a radial error less than the quoted radial accuracy 95 percent of the time. Figure 15 plots the cumulative probability for radial error based upon the simulation data. Following this standard, radial accuracy for this system is 90 meters.

The complex calculations associated with a Kalman smoother make it important to compare the performance of the smoother against a single pass Kalman filter. A small improvement in tracking performance may not justify the additional computational loading needed to smooth the data. The output of the extended Kalman filter operating forward in time is compared with the final smoothed values. Figure 16 shows the cumulative radial error distributions for both the filter and the smoother. At the 95 percent level, the forward filter has a STANAG 4278

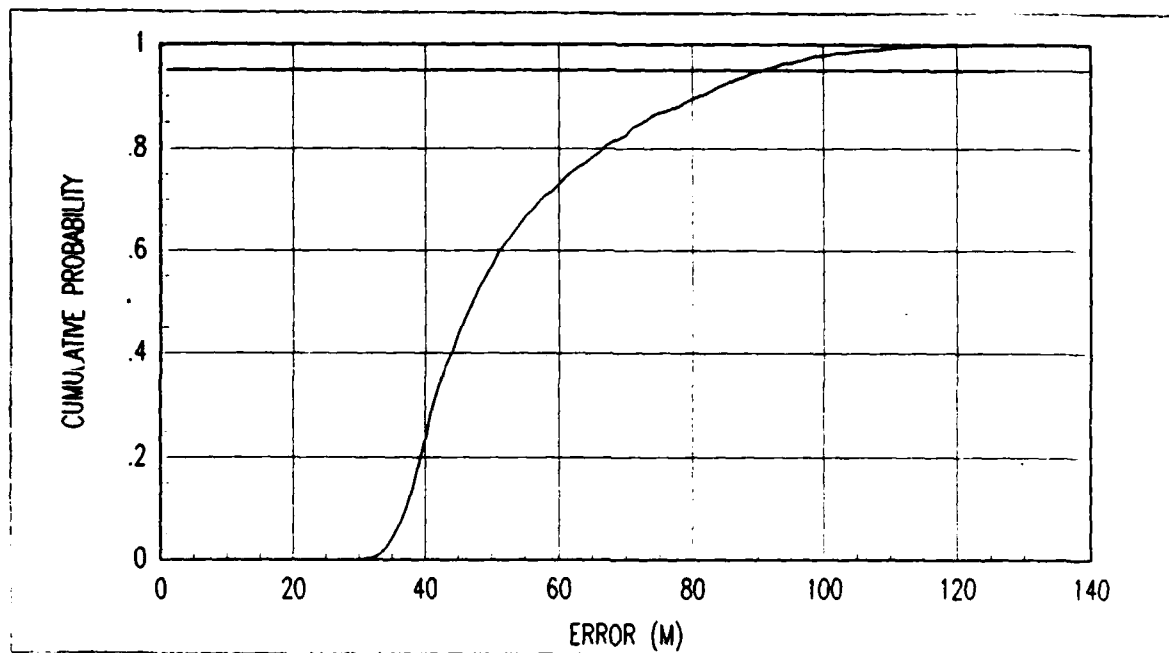


Figure 15. Single Smoother Radial Error Cumulative Distribution

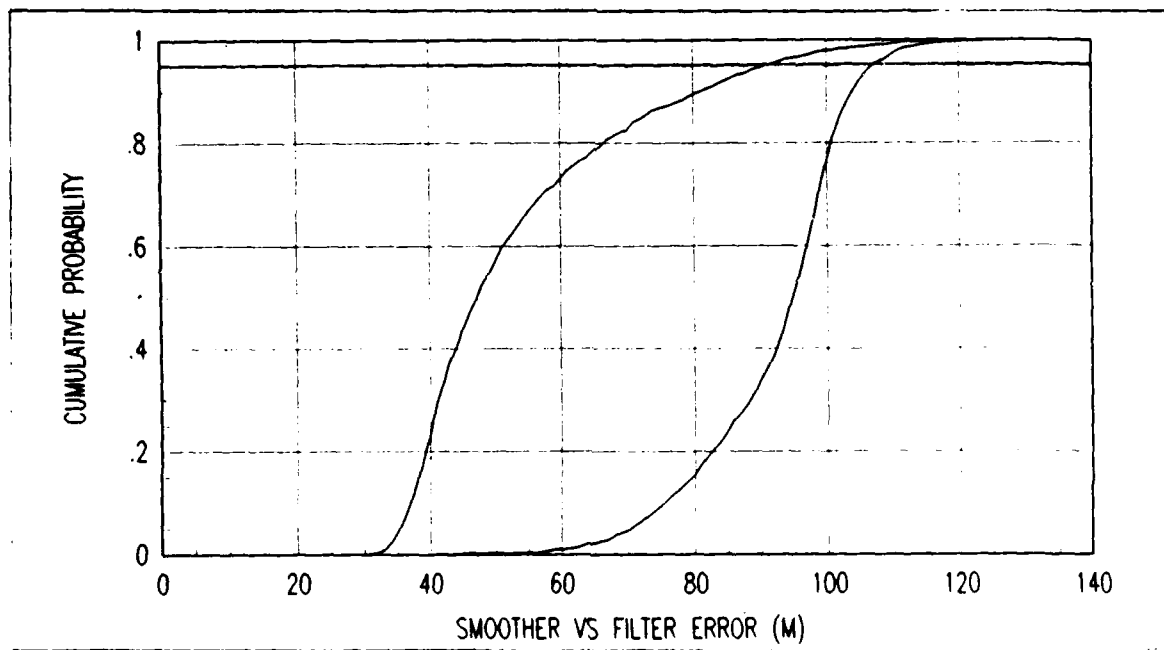


Figure 16. Smoother and Forward Filter Cumulative Error Distributions

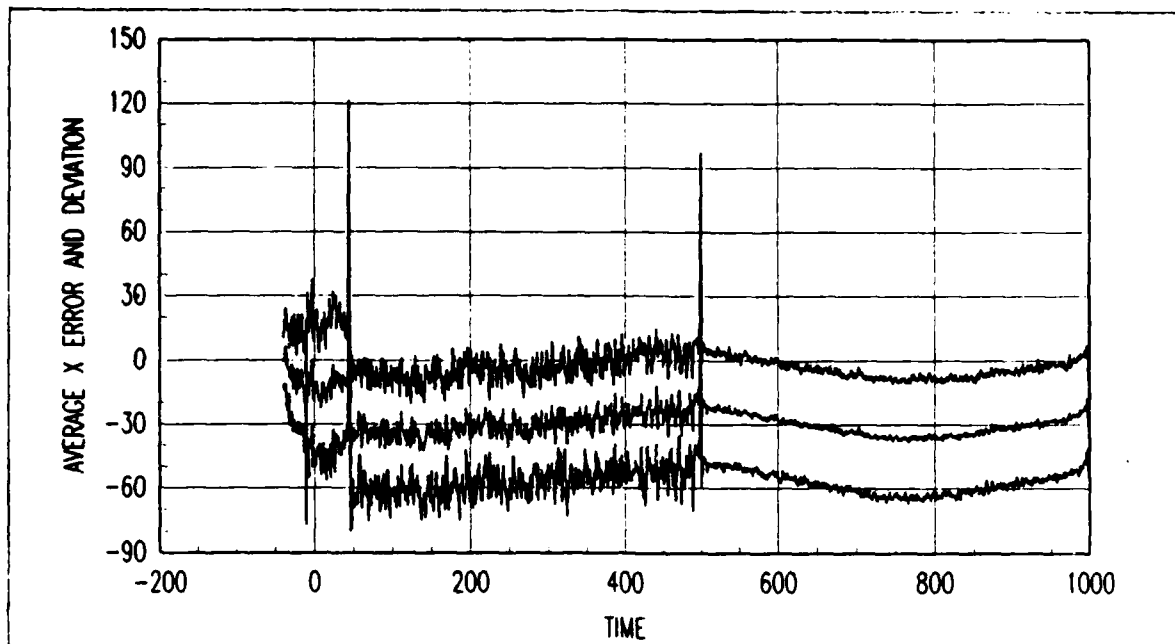


Figure 17. Monte Carlo Results in X Direction

accuracy of 109 meters compared with the 90 meter accuracy for the full smoother.

**5.3.2 Monte Carlo Results** A total of 11 Monte Carlo runs were conducted. Each Monte Carlo run processes a different corrupted version of the same aircraft trajectory. The mean and standard deviation of  $\hat{P}_x$ ,  $\hat{P}_y$  and  $\hat{P}_z$  are calculated for the 11 values at each sample period. Figures 17-19 show the mean plus or minus one standard deviation throughout the flight. The jumps that occur in these plots at times  $t = -10$ ,  $t = 45$ ,  $t = 200$  and  $t = 500$  seconds correspond to TACAN beacon changes. Changing TACAN beacons also causes changes in solution geometry.

Using the eleven Monte Carlo values for radial error at each sample period, the mean and the mean plus or minus one standard deviation are calculated and plotted in Figure 20. Figure 21 shows the cumulative distribution of the radial error for the Monte Carlo runs. The 95 percent accuracy figure for this system is 135 meters.

Changing aircraft position along with changing TACAN beacon geometry was shown earlier to cause large changes in the smoother performance. This bimodal nature of the radial error cumulative distribution also demonstrates this effect.

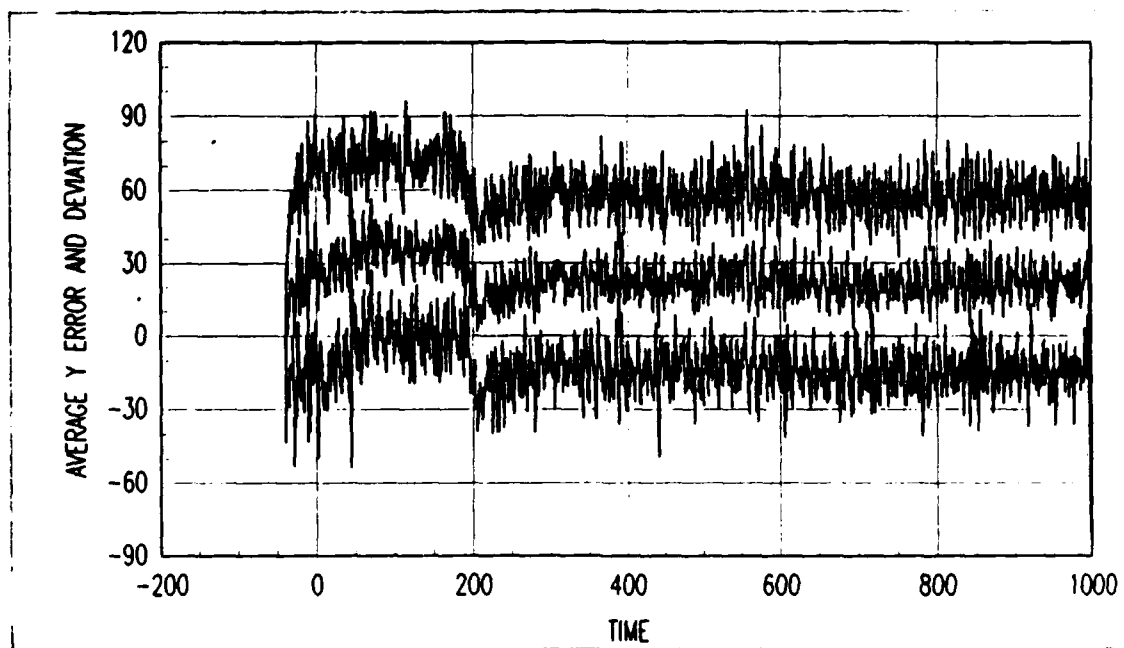


Figure 18. Monte Carlo Results in Y Direction

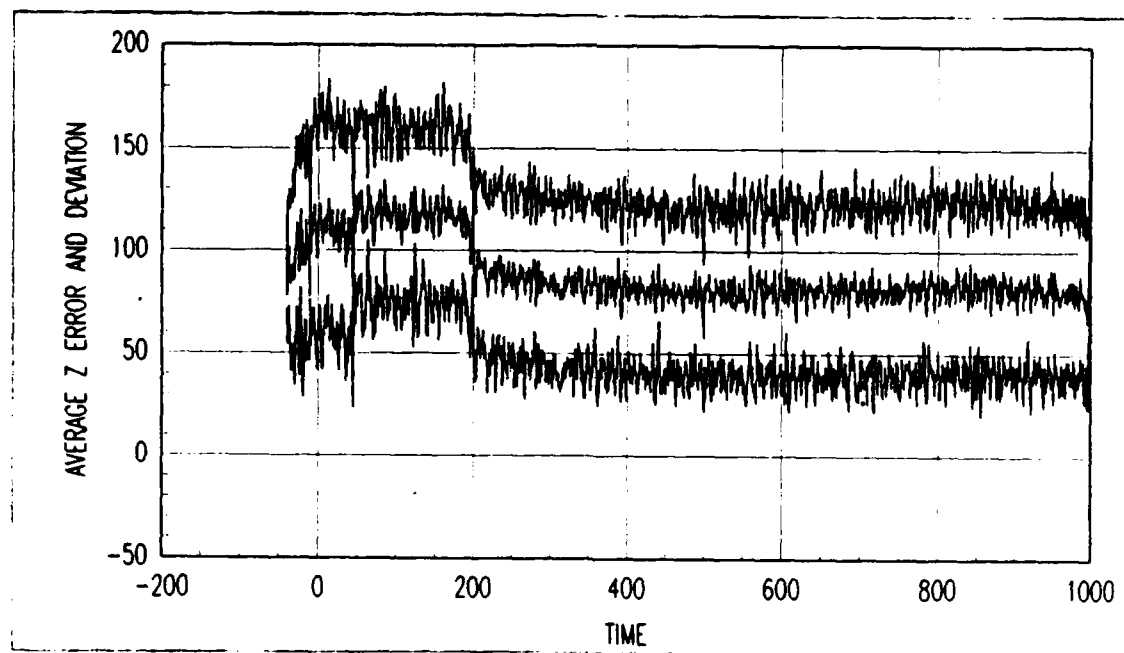


Figure 19. Monte Carlo Results in Z Direction

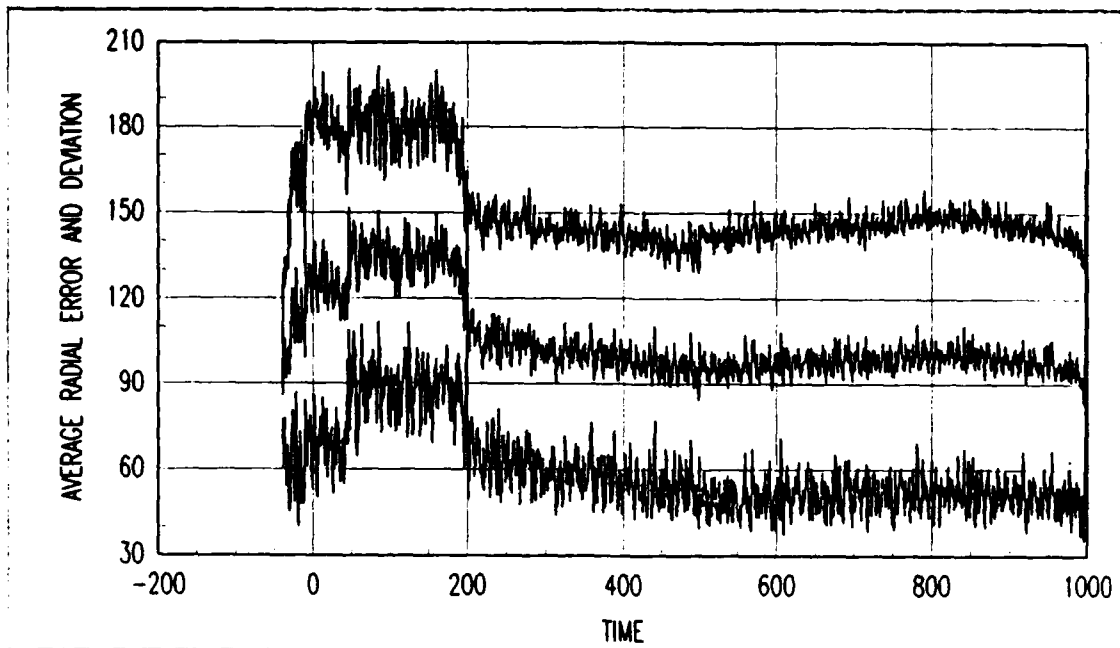


Figure 20. Monte Carlo Radial Error

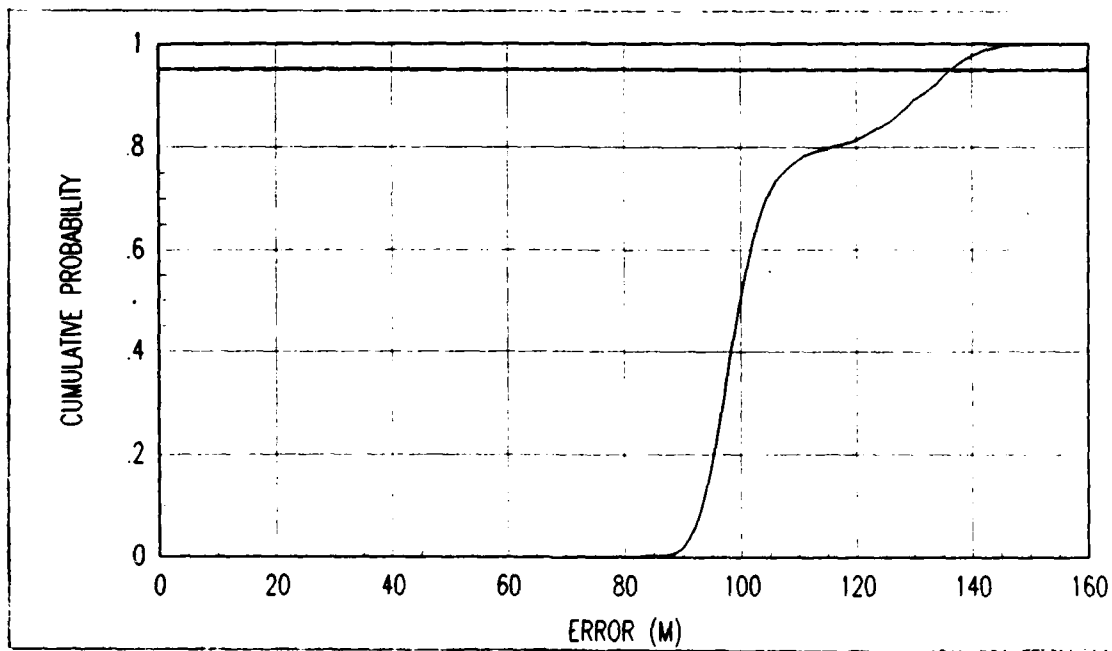


Figure 21. Cumulative Distribution of Monte Carlo Radial Error

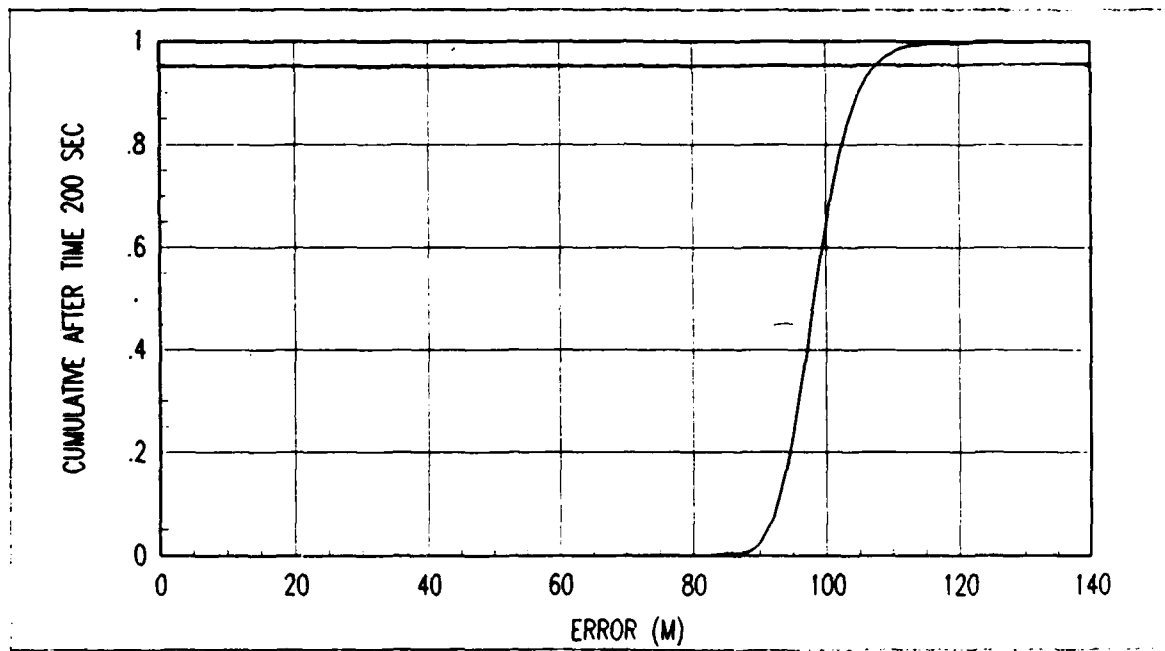


Figure 22. Cumulative Distribution after  $t = 200$  seconds

Considering only the values after the TACAN change at time  $t = 200$  seconds gives the cumulative distribution shown in Figure 22. The system achieves an accuracy of 109 meters from  $t = 200$  seconds through the end of the flight at  $t = 1000$  seconds.

## *VI. Conclusions and Recommendations*

### *6.1 System Accuracy*

Performance of this tracking system meets the desired accuracy specifications. During the computer simulations, the system placed the aircraft within 135 meters of its true position 95 percent of the time. The system does not have any difficulty tracking the aircraft through accelerations, decelerations, ascents, descents or turns.

### *6.2 Recommendations*

The tracking system developed in this thesis cannot satisfy the requirements of all test programs, but it does offer a low-cost alternative to flying at an instrumented test range. This method is adequate for many projects. Other programs requiring more accurate tracking information can use this system to supplement test range flying. It would allow thorough equipment and procedural checkouts for complex programs before spending the time and money to deploy to a range for full-scale testing. The Test Wing should follow up on this project and turn the promise shown in these results into an operational system.

### *6.3 Follow-On Work*

After working on this project, several possible extensions have surfaced that will improve program execution and enhance systems tracking capability.

*6.3.1 Binary Data Files* The program currently does all file manipulations using ASCII data files. These files allow easier program debugging since the VAX text editor can examine or modify the information.

All values are double precision and take up 20 bytes of storage per value. Using binary files in the Fortran code to read and write to disk would decrease

storage requirements to 8 bytes per value, a savings of 60 percent. Along with storage savings, these files allow faster disk reads and writes since fewer bytes are transferred, and the computer does not have to convert between ASCII and internal floating representations.

**6.3.2 Adaptive Extended Kalman Filter** The current tracking system uses a 15-state extended Kalman filter. Five of those states estimate essentially constant values. A 10-state adaptive Kalman filter using those bias values as parameters can provide similar tracking performance. The lower dimensionality of the extended filter decreases system storage requirements and allows faster processing of measurements.

**6.3.3 Factored Filter** The current filter performs full-state estimation using the standard equations for an extended Kalman filter. To avoid numerical difficulties that can arise in the filter equations, all calculations use double precision variables on the computer. By recoding the filter using the UD factored form, most of these operations can be done using single precision math [34:392].

**6.3.4 Fine Tuning** The lack of dual TACAN data collected in the real world does not make it worthwhile to expend a lot of effort in tuning the  $\mathbf{Q}$  and  $\mathbf{R}$  matrices used by the Kalman filter. When the Test Wing has this data available, then the filter should be tuned to make allowances for unmodelled effects that may corrupt the measurement signals. Another approach to tuning the filter would involve developing higher order truth models that better represent real world data.

**6.3.5 Integration With Wing Data Collection and Reduction** Test data formats often vary from one program to the next. Working with the Test Wing data analysts and instrumentation personnel to define standards for using this system will avoid wasted time and effort in the future. These standards should include:

- an equipment package for installation on the test aircraft
- guidelines for selecting TACAN beacons during a test mission
- in-flight operating procedures for the TACAN transceivers
- automating the procedures for converting raw dual TACAN data into tracking data

**6.3.6 Multiple Sensor Integration** This research effort concentrated on the measurements available in a minimally equipped aircraft. Many Wing test programs use additional on-board navigation equipment, such as INS, GPS and long range navigation (LORAN). Developing a Kalman filter or filter to integrate these various measurement sources will allow development of a more complex, and hopefully more accurate, tracker.

## Bibliography

1. Bate, Roger R., Donald D. Mueller and Jerry E. White. *Fundamentals of Astrodynamics*. New York: Dover, 1971.
2. Berg, Russell F. "Estimation and Prediction for Maneuvering Target Trajectories." *IEEE Transactions on Automatic Control*, AC-28:294-304, March 1983.
3. Bierman, Gerald J. and Catherine L. Thorton. "Numerical Comparison of Kalman Filter Algorithms: Orbit Determination Case Study." *Automatica*, 13:23-35. Pergamon Press, 1977.
4. Britting, Kenneth R. *Inertial Navigation Systems Analysis*. New York: John Wiley and Sons, Inc, 1971.
5. Broughton, D. W. "Standardization Within NATO on the Method of Expressing Navigation Accuracies." *Navigation: Journal of The Institute of Navigation*, 33:83-89 (Summer 1986).
6. Chang, Chaw-Bing, and John A. Tabaczynski. "Application of State Estimation to Target Tracking." *IEEE Transactions on Automatic Control*, AC-29:98-109 (February 1984).
7. Colin, Robert I. and Sven H. Dodington. "Principles of TACAN." *Electrical Communication*, 11-59, March 1956.
8. Collins Avionics Group. "Prime Item Development Specification for Receiver-Transmitter, Radio RT-1159/A." Contract Number F19628-75-C-0144, 1 July 1977.
9. Cook, Charles E. "Radio Communication and Navigation in the Presence of Linearly Distributed Noise Sources." *Navigation: Journal of The Institute of Navigation*, Volume 32, Number 2, pp158-168, Summer 1985.
10. Cubic Corporation. "ASPMS Tracking Filter." Unpublished article.
11. Cubic Corporation. "Computer Program Development Specification for Aircraft Space Position Measurement System (ASPMS)." Contract Number F33615-74-C-0142, 2 June 1976.
12. Data Reduction and Computing Working Group. "Error Analysis and Methods for Estimating Errors in Position, Velocity, and Acceleration Data." Document 119-71, pp59-67.
13. Faridani, Hamid M. "Performance of Kalman Filter with Missing Measurements." *Automatica*, Volume 22, Number 1, pp117-120, 1986.
14. Franzen, John. "Radar Accuracy for Horizontal Plane FPS-16." Unpublished paper, 4950TESTW/FFTA, Wright-Patterson AFB, OH, 20 July 1987.

15. Franzen, John. "DME Three-Station Linear Error Analysis." Unpublished paper, 4950TESTW/FFTA, Wright-Patterson AFB, OH.
16. Franzen, John. "Calibration of Dual-DME Positioning System." Unpublished paper, 4950TESTW/FFTA, Wright-Patterson AFB, OH, October 1987.
17. Franzen, John. "Description of the MARK XV Flight Test DME/DME Position Fixing Algorithm." Unpublished paper, 4950TESTW/FFTA, Wright-Patterson AFB, OH, 1987.
18. Franzen, John. "TRW Algorithm." Unpublished paper, 4950TESTW/FFTA, Wright-Patterson AFB, OH.
19. Fried, W. R. "A Comparative Performance Analysis of Modern Ground-Based, Air-Based, and Satellite-Based Radio Navigation Systems." *Navigation: Journal of The Institute of Navigation*, 24:48-58 (Spring 1977).
20. Fulghum, David. "New Satellites to Guide B-2 Crews, Civilians." *Air Force Times*, 28 November 1988.
21. Gideon, Francis C. "Thesis Topic Proposal for Electrical Engineering Student" Official Letter, 4950 Test Wing, Wright-Patterson AFB, OH, 15 December 1987.
22. Groginsky, Herbert L. "Position Estimation Using Only Multiple Simultaneous Range Measurements." *IRE Transactions on Aeronautical and Navigational Electronics*, 178-187, September 1960.
23. Hurrass, Kerlheinz. "Avionics Flight Evaluation System (AFES)." Deutsche Forschungs - und Versuchsanstalt fur Luft - und Raumfahrt e. V. (DFVLR), Institut fur Flugfuhrung, Germany.
24. Kalman, R. E. "A New Approach to Linear Filtering and Prediction Problems." *Journal of Basic Engineering*, pp35-45, March 1960.
25. Laurila, Simo. *Electronic Surveying and Mapping*. Institute of Geodesy, Photogrammetry and Cartography, The Ohio State University, 1960.
26. Latham, R. "Aircraft Positioning with Multiple DME." *Navigation: Journal of The Institute of Navigation*, 21:150-158 (Summer 1974).
27. Latham, R. W. and P. T. Richards. "A Multi-DME/Inertial System for Aircraft Positioning." *Navigation: Journal of The Institute of Navigation*, 24:72-83 (Spring 1977).
28. Latham, R. W. and R. S. Townes. "DME Errors." *Navigation: Journal of The Institute of Navigation*, 23:332-342 (Winter 1975-76).
29. Lee, B. "A Scheme for Estimating Aircraft Velocity Directly from Airborne Range Measurements." *Navigation: Journal of The Institute of Navigation*, 20:29-40 (Spring 1973).

30. Leenhouts, Pieter P. "On the Computation of Bi-Normal Radial Error." *Navigation: Journal of The Institute of Navigation*, 32:16-28 (Spring 1985).
31. Logue, Thomas V. "An Analysis of Radio Navigation Sensor Accuracies Associated with Area Navigation (RNAV)." Report Number FAA-RD-78-85, Systems Research and Development Service, Federal Aviation Administration, Washington D.C., August 1978.
32. Maybeck, Peter S. "Filter Design for a TACAN-Aided Baro-Inertial System with ILS Smoothing Capability." AFFDL-TM-74-52, Air Force Flight Dynamics Laboratory, Wright-Patterson AFB, OH, 1974.
33. Maybeck, Peter S. "Kalman Filtering: Concepts, Design and Extensions." Lecture Notes, Air Force Institute of Technology, September 1983.
34. Maybeck, Peter S. *Stochastic Models, Estimation, and Control Volume 1*. New York: Academic Press, 1979.
35. Maybeck, Peter S. *Stochastic Models, Estimation, and Control Volume 2*. New York: Academic Press, 1982.
36. Maybeck, Peter S. *Stochastic Models, Estimation, and Control Volume 3*. New York: Academic Press, 1982.
37. Maybeck, Peter S. Personal Interviews, June-August 1988.
38. Maybeck, Peter S. and William H. Worsley and Patrick M. Flynn. "Investigation of Constant Turn-Rate Models in Filters for Airborne Vehicle Tracking." *Proceedings of NAECON 1982*, 2:896-903 (May 1982).
39. McCormack, Christopher J. "TACAN/INS Performance Evaluation (TIPE) Flight Test Report." 4950-TR-86-10, 4950th Test Wing, Wright-Patterson AFB, OH, January 1987.
40. Musick, S. "PROFGEN — A Computer Program for Generating Flight Profiles." Technical Report AFAL-TR-76-247, Air Force Wright Aeronautical Laboratories, Wright-Patterson AFB, OH, November 1976.
41. Naimo, Matthew. "Aircraft Tracking and Data System (ATADS) Position Accuracy." Technical Note DOT/FAA/CT-TN83/35, Federal Aviation Administration, Atlantic City Airport, NJ, December 1983.
42. Naimo, Matthew. "Test and Evaluation of Remote Area Precision Positioning System (RAPPS) Phase 1." Report Number FAA-RD-80-102, Federal Aviation Administration, Washington D.C., March 1981.
43. O'Conner, John J. "Methods of Trajectory Mechanics." Report Number ESMC-TR-80-45, Eastern Space and Missile Center, Patrick AFB, FL, May 1981.

44. Perrett, Edouard E. "Error Analysis for Determination of Target Position and Velocity From Two or More Observers." WADD Technical Note 60-70, Wright Air Development Division, Wright-Patterson AFB, OH, June 1960.
45. Rawlings, R. C. "Flight Assessment and Operation of Improved Navigation Systems." Royal Aircraft Establishment Technical Memorandum FS 234, April 1980.
46. Rawlings, R. C. and Harlow, R. A. "Flight Trials to Determine the Overall System Performance of Distance Measuring Equipment." Royal Aircraft Establishment Technical Report 79140, November 1979.
47. Riggins, Robert N. "A Design of a Trajectory Estimator Using Multiple DME Range Measurements." Master's Thesis, AFIT/GCE/EE/78-4, Air Force Institute of Technology, Wright-Patterson AFB, OH, March 1978.
48. Sampson, Stephen R. "A Survey of Commercially Available Positioning Systems." *Navigation: Journal of The Institute of Navigation*, 32:139-148 (Summer 1985).
49. Scheder, Robert A. "A Computer Program for Double Sweep Optimal Smoothing." AMSAA-TR-246, US Army Material Systems Analysis Activity, Aberdeen Proving Ground, MD, January 1979.
50. Scheder, Robert A. "A Self-Adapting Target State Estimator." US Army Material Systems Analysis Activity, Aberdeen Proving Ground, MD, 1976.
51. Solomon, Joseph K. and Robert J. Urbanic. "A Navigation Covariance Performance Analysis Package MSOFE and PROFGEN." Final Report, EENG 735, Air Force Institute of Technology, June 1988.
52. Sorenson, H. W. "Least-Squares Estimation: From Gauss to Kalman." *IEEE Spectrum*, 7:63-68 (July 1970).
53. Spilker, Robert S. "Addendum to the Block 4 Computer Program Development Specification (CPDS) for the Airborne Digital Avionics Test System (ADATS) Mission Software (AMS) for Block 5." TRW Dayton Engineering Laboratory, Dayton, OH, September 1985.
54. Symbolics, Inc. *VAX/UNIX Macsyma Program Reference Manual Version 11*. USA, 1985.
55. Verhaegen, Michel and Paul van Dooren. "Numerical Aspects of Different Kalman Filter Implementations." *IEEE Transactions on Automatic Control*, AC-31:907-917 (October 1986).

*Vita*

Christopher Joseph McCormack was born on [REDACTED]

[REDACTED] He graduated from high school in 1980 and attended the United States Air Force Academy. He graduated from the Air Force Academy in May of 1984 with a Bachelor of Science degree in Electrical Engineering and a commission as a second lieutenant in the Air Force. He served as a test director and test project manager in the Electronic Combat Division of the 4950th Test Wing at Wright-Patterson AFB, OH from July of 1984 until entering the Air Force Institute of Technology School of Engineering in June of 1987. He is a member of Eta Kappa Nu and Tau Beta Pi.

[REDACTED]

**REPORT DOCUMENTATION PAGE**

1a. REPORT SECURITY CLASSIFICATION <b>UNCLASSIFIED</b>		1b. RESTRICTIVE MARKINGS	
2a. SECURITY CLASSIFICATION AUTHORITY		3. DISTRIBUTION/AVAILABILITY OF REPORT <b>Approved for Public Release; Distribution Unlimited</b>	
2b. DECLASSIFICATION/DOWNGRADING SCHEDULE			
4. PERFORMING ORGANIZATION REPORT NUMBER(S) <b>AFIT/GE/ENG/88D-28</b>		5. MONITORING ORGANIZATION REPORT NUMBER(S)	
6a. NAME OF PERFORMING ORGANIZATION <b>School of Engineering</b>		6b. OFFICE SYMBOL <i>(If applicable)</i> <b>AFIT/ENG</b>	7a. NAME OF MONITORING ORGANIZATION
6c. ADDRESS (City, State, and ZIP Code) <b>Air Force Institute of Technology (AU) Wright-Patterson AFB, OH 45433-6583</b>		7b. ADDRESS (City, State, and ZIP Code) <i>Received 15-Jan-89</i>	
8a. NAME OF FUNDING/SPONSORING ORGANIZATION <b>Flight Test Directorate</b>		8b. OFFICE SYMBOL <i>(If applicable)</i> <b>4950TESTW/FF</b>	9. PROCUREMENT INSTRUMENT IDENTIFICATION NUMBER <i>18</i>
8c. ADDRESS (City, State, and ZIP Code) <b>Wright-Patterson AFB, OH 45433-6513</b>		10. SOURCE OF FUNDING NUMBERS	
		PROGRAM ELEMENT NO.	PROJECT NO.
		TASK NO.	WORK UNIT ACCESSION NO.
11. TITLE (Include Security Classification) <b>Aircraft Tracking With Dual TACAN</b>			
12. PERSONAL AUTHOR(S) <b>Christopher J. McCormack, B.S., Captain, USAF</b>			
13a. TYPE OF REPORT <b>M.S. Thesis</b>	13b. TIME COVERED FROM _____ TO _____		14. DATE OF REPORT (Year, Month, Day) <b>1988 December</b>
15. PAGE COUNT <b>68</b>			
16. SUPPLEMENTARY NOTATION			
17. COSATI CODES		18. SUBJECT TERMS (Continue on reverse if necessary and identify by block number) <b>DME, TACAN, Automatic Tracking, TSPI, Navigation, Radionavigation, Kalman Filter, Kalman Smoother</b>	
FIELD <b>17</b>	GROUP <b>07</b>	SUB-GROUP <b>03</b>	
01	04		
19. ABSTRACT (Continue on reverse if necessary and identify by block number)  This thesis addresses the problem of determining aircraft position during flight given noisy and biased measurements from a barometric altimeter and two tactical air navigation (TACAN) transceivers.  A Kalman smoother is developed to perform post-flight data processing on the measurement data. The smoother estimates aircraft position, velocity, and acceleration as well as biases in the measurements.  Since actual flight test data is not available, computer simulations examine the performance of this tracking technique. The simulated flight includes low and high-speed turns, constant rate ascents, descents, and accelerations. The tracking algorithm tracked the aircraft to within 135 meters of its actual position 95 percent of the time. An unaided inertial navigation system used by the 4950th Test Wing in another flight test program showed a position error growth rate of 2000 meters per hour.			
20. DISTRIBUTION/AVAILABILITY OF ABSTRACT <input checked="" type="checkbox"/> UNCLASSIFIED/UNLIMITED <input type="checkbox"/> SAME AS RPT. <input type="checkbox"/> DTIC USERS		21. ABSTRACT SECURITY CLASSIFICATION <b>UNCLASSIFIED</b>	
22a. NAME OF RESPONSIBLE INDIVIDUAL <b>Robert Williams, Associate Professor</b>		22b. TELEPHONE (Include Area Code) <b>(513) 255-6027</b>	22c. OFFICE SYMBOL <b>AFIT/ENG</b>